NILU: OR 11/98

Modelling of heterogeneous chemistry in the stratosphere

Inga Fløisand

Contents

2

Abstract

A photochemical trajectory model for the stratosphere has been employed at NILU over several years. The model consists of several modules describing photodissociation, gas phase chemistry, microphysical processes leading to liquid and solid particle formation, and heterogeneous chemical reactions facilitated by particles. The modules are coupled so that the processes are subject to mutual interactions in an air parcel following isentropic trajectories over 10-day periods. The model includes 58 chemical species and six families of species. Photo-dissociation rates are calculated using a two-stream approximation for the calculation of radiative transfer. The microphysical module describes the formation and evolution of liquid sulphuric acid and ternary solution particles as well as solid phase particles on the basis of temperature, pressure and the gas phase mixing ratio of nitric acid and water. The particles facilitate heterogeneous reactions that activate chlorine and bromine species and convert reactive nitrogen into nitric acid. This report gives a description of the modules and how the processes are parameterised.

In addition, this report includes a study of heterogeneous chemical reactions in connection with liquid sulphuric acid particles. In this study, the full micro-physical scheme is not utilised, and the model has been applied as a box model. The aim is to quantify the impact of liquid phase heterogeneous reactions on in-situ chemical processes and ozone loss at middle and high northern latitudes in the lower stratosphere. A background and a volcanically enhanced particle scenario have been used. The effect of known heterogeneous reactions involving chlorine, bromine and nitrogen reservoir species has been studied. In addition, a proposed reaction for self-activation of chlorine and a mechanism for heterogeneous production of hydrogen peroxide are investigated. The partitioning of species, ozone loss mechanisms and ozone depletion rates are examined and the difference in in-situ column ozone loss resulting from the reactions has been calculated.

4

Modelling of heterogeneous chemistry in the stratosphere

1. Introduction

The main purpose of this report is to present a detailed description of the photochemical trajectory model for the stratosphere which has been used at NILU for several years. The model has been applied in various studies (De Haan et al., 1997; Fløisand et al., 1998; Reid et al., 1998; Galle et al., 1999). In addition, the impact of various heterogeneous reactions in connection with liquid sulphuric acid particles on in-situ chemical ozone loss at middle and high latitudes is investigated. In this study, the model is applied as a box model and the full microphysical scheme has not been utilised as calculations have been made, assuming only liquid sulphuric acid particles, and the uptake of nitric acid and the freezing of particles has been omitted.

The results from investigations performed with the photochemical trajectory model within the frame of two projects are presented. The project "Laboratory studies and modelling of heterogeneous chemistry in the stratosphere (LAMOCS)", funded by the European Commission, was a joint laboratory and modelling study of heterogeneous chemical processes which take place on the stratospheric sulphuric acid aerosol. The aim was to study the influence of such processes on the partitioning of hydrogen, halogen and nitrogen species in the lower stratosphere over middle to high northern latitudes. One of the main tasks was modelling studies of the impact of heterogeneous chemical reactions on stratospheric ozone depletion. Some potentially important heterogeneous reaction schemes that could take place in connection with stratospheric sulphuric acid aerosols were suggested. The aim of the second project "Model studies of ozone depletion at high- and mid- northern latitudes", funded by the Research Council of Norway, was to study the heterogeneous interaction of nitrogen, chlorine and bromine compounds with particles. The main emphasis was placed on bromine chemistry.

Heterogeneous reactions play an important role in chemical ozone depletion in the stratosphere. Reservoir species are activated through heterogeneous reactions and subsequent photolysis, followed by catalytic ozone destruction. Both liquid and solid particles can facilitate heterogeneous reactions. The occurrence and abundance of the different types of particles is strongly dependent on in-situ temperature and temperature history, and the concentration of gas phase nitric acid and water vapour. In this study, the role and characteristics of heterogeneous reactions in connection with liquid sulphuric acid particles are studied.

Several reactions involving chlorine, bromine and nitrogen species have been found to take place in the presence of liquid particles (Ravishankara et al., 1999). Some of these reactions take place in the bulk of the particle in the liquid phase. As the temperature decreases, the droplets take up more water, which in turn causes them to swell and the concentration of sulphuric acid to decrease. The solubility of the reactants and thereby the reactive uptake coefficients are enhanced under such conditions. Other heterogeneous reactions have been found

to take place mainly on the surface of the particles, in which case the reactive uptake coefficients are largely temperature independent. However, the increase in surface area density at low temperatures results in enhanced reaction rate coefficients. Heterogeneous reactions may therefore, to a varying degree, influence the partitioning of active and inactive species as a function of temperature. The abundance of liquid sulphuric acid particles is enhanced by volcanic eruptions.

Over the last decades, a decline in total ozone column amounts has been observed at middle latitudes (Harris et al., 1995; Bojkov et al., 1999). This decrease is most evident during the winter and spring months, but a downward trend is also observed during the summer and autumn seasons. The main contribution to middle latitude column ozone decline comes from decreases in the lower stratosphere around 20 km (Ravishankara et al., 1999). However, quantification of the different processes contributing to this depletion is not complete. The region is influenced both by in-situ chemical ozone loss, enhanced by volcanic particles, and by transport from other regions. Erosion of the polar vortex transports air from the outer regions of the vortex to lower latitudes. Both large-scale disturbances and small-scale filamentation can cause exchange of vortex and extra-vortex air. Chemically activated vortex air exposed to sunlight at middle latitudes can lead to local ozone loss (e.g. Reid et al., 1998). Also post-vortex ozone dilution can have an impact on middle latitude ozone abundance. Reverse domain-filling trajectory calculations show that approximately one third of the observed change in total ozone at 30-60°N from May 1979 to May 1997 could be caused by dilution after the break-up of the vortex in spring (Knudsen et al., 1998). This indicates that dilution plays an important role in spring and summer at middle latitudes.

However, the vertical, latitudinal and seasonal characteristics of the middle latitude depletion of ozone indicate that the major contribution comes from in-situ chemical processing. The temperature at middle and low latitudes is usually too high for solid particles to form, and liquid particles are the only available reaction sites for heterogeneous reactions. Numerical model simulations have shown that heterogeneous activation on volcanically enhanced sulphuric acid aerosols could decrease the ozone abundance at middle latitudes (e.g. Hofmann and Solomon, 1989; Pitari and Rizi, 1993; Bekki and Pyle, 1994; Tie et al., 1994; Solomon et al. 1996). These results are supported by observations of ozone and nitrogen compounds after the Mt. Pinatubo eruption in 1991 (e.g. Johnston et al., 1992; Gleason et al., 1993; Koike et al., 1994; Rinsland et al., 1994). In order to reproduce not only the timing, but also the magnitude of the observed ozone following volcanic eruptions, small scale temperature variability combined with changes in aerosol and chlorine abundance must be taken into account (Solomon et al., 1998). Apart from the enhancement in liquid sulphuric acid aerosols caused by major volcanic eruptions, balloon-borne (Hofmann, 1990) and satellite observations (Hitchman et al., 1994; Thomason et al., 1997a) indicate that the stratospheric aerosol abundance in general has increased over the last decades.

In the Arctic region, significant ozone depletion has taken place during winter and early spring over the last years (e.g. European Commission, 1997 and references therein; Manney et al., 1996; Rex et al., 1997). The depletion is, however, not of the same magnitude as over the Antarctic. The conditions for the formation of solid Polar Stratospheric Cloud (PSC) particles are not as favourable as in the Antarctic, and heterogeneous activation on liquid particles likely plays an

important role in Arctic ozone depletion. Liquid particle heterogeneous activation can persist during periods with warmer temperatures and these particles may play an important role in halogen activation in spring. The chlorine activation in or on liquid particles is correlated with decreasing temperature and the rate coefficients are comparable to those on PSCs at temperatures where such particles can exist (Ravishankara et al., 1999). Temperature is therefore the most important parameter in controlling heterogeneous chlorine activation.

In addition to the winter and spring time decline in ozone observed at high latitudes, regions of low stratospheric ozone have been observed in the Arctic and Antarctic during summer (e.g. Park and Russell, 1994). The low ozone concentrations are found between 20 and 30 km, poleward of ~60°. During summer, the ozone concentration in this region is dominated by chemistry (Perliski et al., 1989). Model calculations performed by Brühl et al. (1998) show that the observed summertime low ozone is due to catalytic destruction by nitrogen oxides. However, model calculations performed by Randeniya et al. (1997) have shown that heterogeneous reactions on liquid sulphuric acid particles could lead to substantial ozone depletion at high latitudes in summer.

The photochemical trajectory model used in this study takes into account gas phase chemical reactions, photodissociation and heterogeneous reactions. The present study has been conducted as a box model study at middle and high latitudes in the lower stratosphere in order to quantify in-situ chemical ozone loss attributed to different chemical processes. The impact of adding several individual heterogeneous reactions facilitated by liquid sulphuric acid particles on the partitioning of species, and the relative importance of the different ozone loss mechanisms have been studied. In addition, the effect on ozone depletion rates and column abundance has been quantified. The main focus has been placed on the latitudinal, altitudinal and seasonal variation of the reactions based on a scenario with volcanically enhanced liquid sulphuric acid particles.

The first part of this report describes the photochemical trajectory model. The experimental conditions are defined, followed by results and discussion from simulations of several different heterogeneous reaction schemes. The last part contains a summary and the conclusions.

2. The photochemical trajectory model

The photochemical trajectory model consists of coupled modules describing different atmospheric processes. Ch. 2.1 gives an outline of the types of problems that can be addressed by this model, the assumptions that are made, the limitations and uncertainties. A description of the calculations of solar fluxes and photodissociation coefficients is given in Ch. 2.2, and calculations of the evolution of liquid and solid particles is described in Ch. 2.3. The numerical scheme, gas phase reactions, heterogeneous reactions, and initialisation of chemical species are described in Ch. 2.4. Ch. 2.5 describes the movement of air parcels and the calculation of mean temperature used in the box model simulations. Finally, the presentation of model results is described in Ch. 2.6.

8

2.1 Scope of model

The photochemical trajectory model describes the evolution of chemical species and particles in a dimension-less box, which is advected along a trajectory according to the wind field. There is no exchange of matter with the surrounding air and the evolution is therefore solely dependent on the initial conditions and the changing solar radiation, pressure and temperature along the air parcel trajectory.

The box follows isentropic air parcel trajectories calculated on the basis of observed wind fields. The isentropic assumption is only valid for a limited time period, and the air parcel trajectories are therefore calculated for 10 days. The model has been used for several studies in this mode (De Haan et al., 1997; Fløisand et al., 1998; Reid et al., 1998; Galle et al., 1999). Providing there are meteorological data available, the photochemical model can be utilised for any geographic area. The model offers limited vertical coverage as calculations are made for isentropic levels for which data are available only on certain levels. In this study, calculations have been made for stationary air parcels at fixed geographical positions.

The computational costs are low for such a simple model, and an extensive chemistry scheme may be included. The model is well suited for studies of the impact of atmospheric conditions on the trace gas composition which can be attributed to specific chemical processes. Sensitivity tests can be performed by altering the parameterisation of certain processes, by adding or omitting reactions or processes, or by changing the initial conditions.

2.2 Solar fluxes and photodissociation coefficients

2.2.1 Solar flux

A simplified short-wave radiation transfer model (Isaksen et al., 1977) is used to calculate solar fluxes and photolysis rates. The calculations of solar flux include molecular scattering, reflection due to the Earth's albedo and absorption by O_2, O_3 and NO_2. The vertical distribution of the total air density and the absorbents O_2, O_3 and NO_2 along the radiation stream are taken from the Oslo 2-D model (Stordal et al., 1985). Solar fluxes are calculated in the spectral region 186-730 nm at height intervals of one kilometre, extending from the ground and up to 50 kilometres.

The total solar radiation (F_i^0) reaching a certain level i, is the sum of the direct incoming solar radiation ($\downarrow F_i^0$) and solar radiation reflected from the Earth's surface ($\uparrow F_i^0$). The superscript 0 denotes direct, non-scattered radiation.

Eq. 1 $F_i^0 = \downarrow F_i^0 + \uparrow F_i^0$

The direct incoming solar flux at a certain wavelength, reaching a height level i, is expressed as the radiation transmitted from the layer above.

Eq. 2 $\downarrow F_i^0 = \downarrow F_{i+1}^0 \cdot e^{-\Delta \tau_{i+1/2}^*}$

Eq. 2, which is based on the Beer-Lambert law, gives the transmitted flux from the level above ($i+1$) to the level we consider (i). $\Delta\tau^*_{i+1/2}$ is the total optical depth in the interval between level i and level $i+1$, and is given by the absorption of O_2, O_3 and NO_2 as well as scattering from air molecules.

The upper boundary condition ($i=51$) for the flux is specified according to observations. The incoming flux reaching a certain height level i ($\downarrow F_i^0$), can be expressed in terms of the incoming flux at the upper boundary ($\downarrow F_{51}^0$) by substituting for $\downarrow F_{i+1}^0$ in Eq. 2.

$$Eq.\ 3 \qquad \downarrow F_i^0 = \downarrow F_{51}^0 \cdot e^{-\sum\limits_{j=i+1}^{51} \Delta\tau^*_{j-1/2}}$$

The reflected direct solar radiation due to the Earth's albedo, reaching the height level i from below ($i-1$) can be expressed equivalently to Eq. 2.

$$Eq.\ 4 \qquad \uparrow F_i^0 = \uparrow F_{i-1}^0 \cdot e^{-\Delta\tau^*_{i-1/2}}$$

An expression for the reflected flux of the direct solar radiation reaching a certain height level can be defined using the surface albedo, A.

$$Eq.\ 5 \qquad \uparrow F_i^0 = \downarrow F_1^0 \cdot A \cdot e^{-\sum\limits_{j=1}^{i-1} \Delta\tau^*_{j+1/2}}$$

The molecular scattering of the wavelengths considered is in the Rayleigh scattering regime. Rayleigh scattering is isotropic, and the calculations are simplified by assuming that half of the radiation is scattered backward and the other half in the forward direction of the beam. Expressions for scattered fluxes of nth order are given by fluxes of lower order ($n-1$). The downward component is the sum of the flux of the order $n-1$ which is scattered downward in the height level above, and the downward flux of the order n scattered at height levels higher up and transmitted from the level directly above. The scattered flux of nth order reaching level i is

$$Eq.\ 6 \qquad \downarrow F_i^n = \left[\frac{1}{2}\left(\downarrow F_{i+1}^{n-1} + \uparrow F_i^{n-1} \right)\left(1 - e^{-\Delta\tau_{i+1/2}} \right) + \downarrow F_{i+1}^n \right] \cdot e^{-\Delta\tau^*_{i+1/2}}$$

$\Delta\tau_{i+1/2}$ is the optical depth given by the absorption of O_2, O_3 and NO_2 in the height interval between i and $i+1$. An expression similar to Eq. 3 can be developed to express the scattered radiation reaching level i from all levels above. The upward component of the scattered flux is obtained in a similar way. The flux of the order n reaching the height level i is given by

$$Eq.\ 7 \qquad F_i^n = \downarrow F_i^n + \uparrow F_i^n$$

Scattered fluxes above the fifth order were found to have negligible effect on the total flux for Rayleigh scattering (Isaksen et al., 1977). The total flux reaching

10

level i is therefore given by the direct incoming and reflected radiation and the scattered radiation.

Eq. 8 $$F_i = F_i^0 + \sum_{n=1}^{5} F_i^n$$

2.2.2 Photodissociation coefficients

Based on the fluxes calculated through Eq. 8, the photodissociation coefficient J_{ci} of a species c at a height level i, over a certain wavelength region is defined as

Eq. 9 $$J_{ci} = \sum_{\lambda=\lambda_1}^{\lambda_2} \sigma_c(\lambda) \cdot \varepsilon_c(\lambda) \cdot F_i(\lambda) \cdot \Delta\lambda$$

$F_i(\lambda)\Delta\lambda$ is the total solar photon flux, $\sigma_c(\lambda)$ the absorption cross section of species c, and $\varepsilon_c(\lambda)$ is the quantum yield for the particular reaction. All values are average values in the spectral interval, $\Delta\lambda$. The spectral region is divided into 130 intervals. In the region between 320 and 730 nm a spectral interval of 5 nm is used, while shorter intervals are used below 320 nm. The photodissociation coefficients at the pressure level of the trajectory are obtained through logarithmic interpolation between the altitude levels directly above and below.

There are 48 photodissociation processes included in the photochemical trajectory model. They are listed in Table A.1 in Appendix A together with the absorption cross sections and the quantum yields, which are chosen according to DeMore et al. (1997).

2.3 Particles

Liquid and solid particles are included in the photochemical trajectory model. The formation, evolution and disintegration of the different types of stratospheric particles is described by a microphysical model (Larsen, 1991; Larsen et al., 1997) which is coupled to the calculation of the chemical species.

2.3.1 Liquid sulphuric acid particles

The surface area density of liquid sulphuric acid particles is initialised from a data set covering the period 1979-1995 (Jackman et al., 1996; Rosenfield et al., 1997). Extinction coefficient measurements from the satellite instruments SAGE (Stratospheric Aerosol and Gas Experiment) I and II, SAM (Stratospheric Aerosol Measurements) II and SME (Solar Mesosphere Explorer) have been converted to surface area densities. The data are interpolated in space and time to obtain a global data set (Jackman et al., 1996; Rosenfield et al., 1997). The latitudinal resolution is 5°, and the altitudinal resolution is 2 km. These average surface areas include both liquid and solid particles, and are given as monthly zonal averages. The extinction is enhanced in the individual measurements during PSC events (e.g. McCormick et al., 1989). However, the inferred particles are assumed to consist of liquid aerosols only, as the error introduced in the monthly mean values is small.
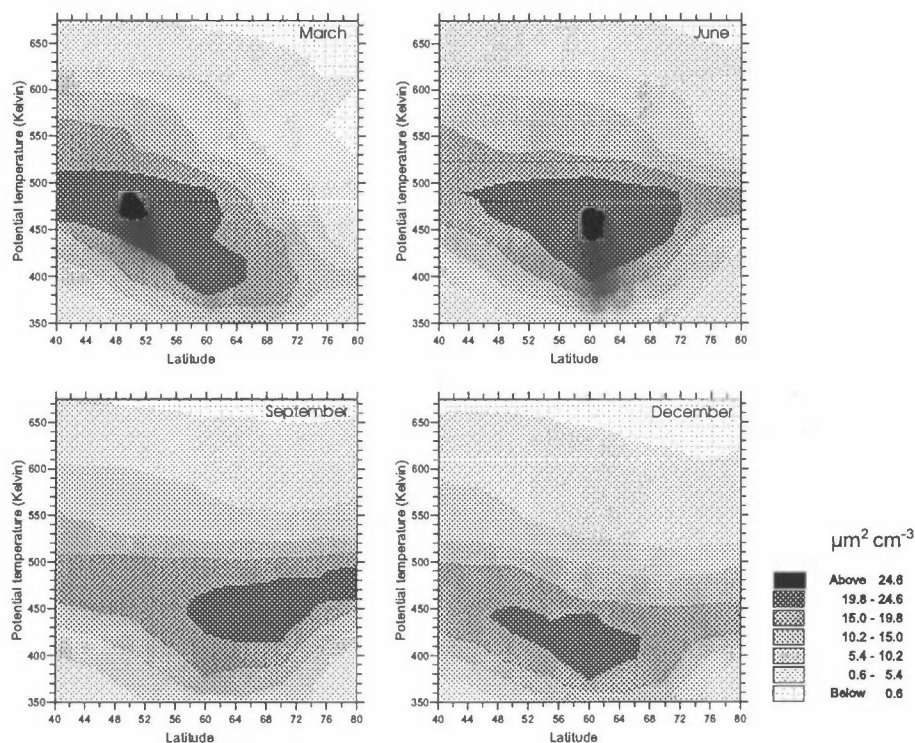
Figure 1: *Monthly mean surface area density of liquid sulphuric acid particles*
(μm^2 cm^{-3}) for 1992 used in the model. Data are shown for March,
June, September and December.

Figure 1 shows the surface area density of liquid sulphuric acid particles as they have been used in this study, with potential temperature as the height co-ordinate. Following the Mt. Pinatubo eruption on 15 June 1991, sulphuric acid particles were distributed throughout the stratosphere. The particles were, however, not present in great amounts at high latitudes above 450 K before after the break-up of the arctic polar vortex at the end of March 1992 (Neuber et al., 1994a; 1994b).

The measurements obtained in 1979 were relatively free of volcanic contribution and may be representative of background sulphuric acid particle levels in the stratosphere (Hofmann, 1990; Thomason et al., 1997b). The maximum surface area density for background conditions is ~1 μm^2·cm^{-3} and is observed in the lower part of the studied altitude region.

2.3.2 Microphysical calculations

The microphysical model (Larsen 1991; Larsen et al., 1997) calculates the formation of, and transition between liquid and solid particles and the scheme is described in Figure 2. The model includes the physical processes of heterogeneous nucleation, condensation, coagulation, evaporation and sedimentation. Sedimentation of particles is not included in the photochemical trajectory model. The liquid particles are basically binary mixtures of water and sulphuric acid (H_2O/H_2SO_4). Under certain conditions the particles will take up nitric acid (HNO_3) and become ternary solutions. There are three types of solid particles. Sulphuric acid tetra-hydrate (SAT, $H_2SO_4 \cdot 4H_2O$) is frozen particles which form as the temperature drops below the SAT formation threshold. Nitric acid
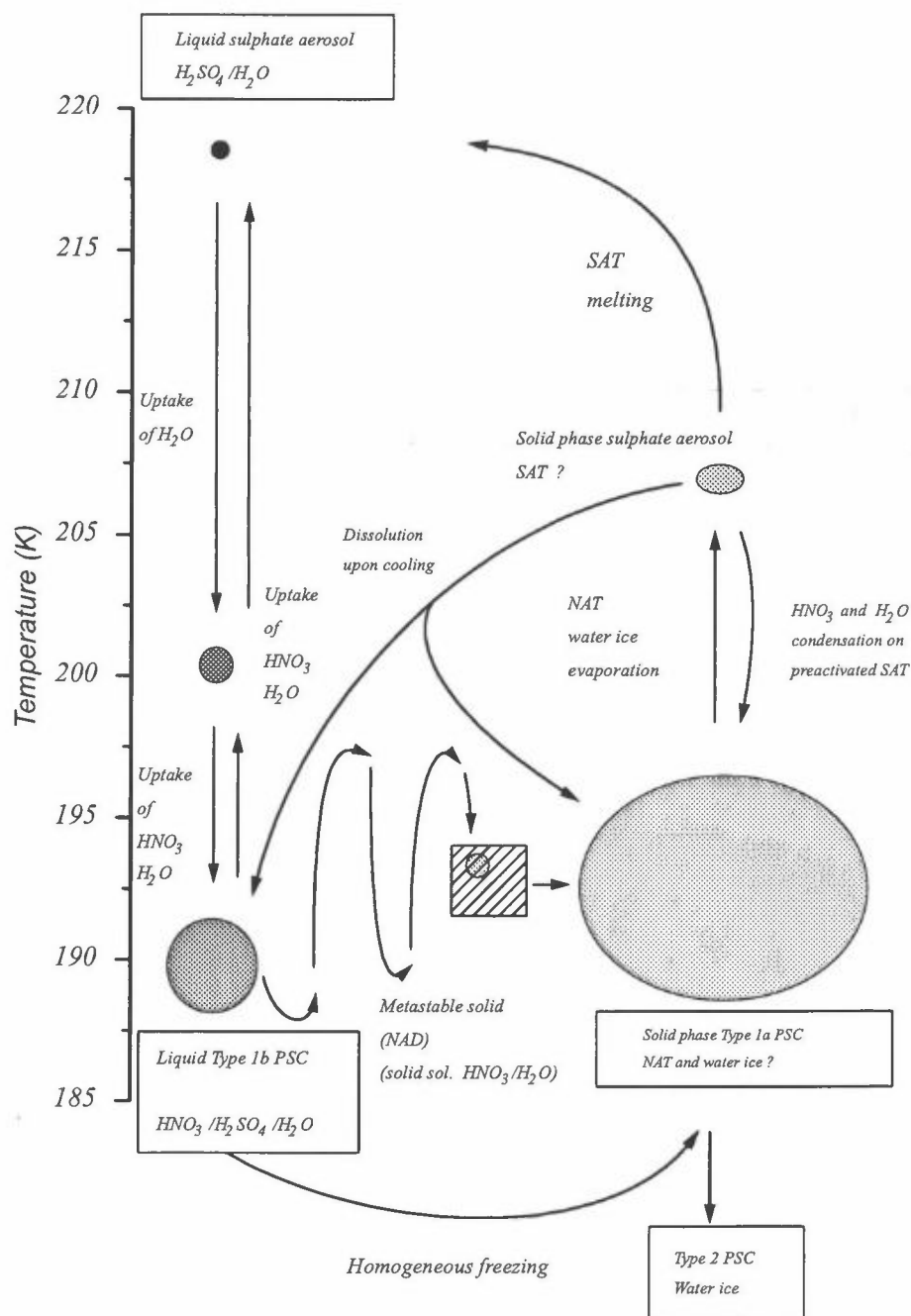
Figure 2: Microphysical scheme, (N. Larsen, personal communication 1999).

trihydrate (NAT, $HNO_3 \cdot 3H_2O$) and ice particles are formed at even lower temperatures. The two latter categories are referred to as Polar Stratospheric Clouds (PSCs), type 1a and type 2, respectively. The liquid ternary solution particles are called PSC type 1b.

The distribution of particle types and sizes is determined by the ambient temperature and pressure as well as the gas phase mixing ratios of HNO_3 and H_2O. The particles are in equilibrium with the ambient air. Thus, HNO_3 and H_2O are removed from the gas phase by condensation and returned upon evaporation. The initial size distribution of sulphuric acid aerosols is assumed to be log-

normal, and is calculated on the basis of the total surface area density derived from satellite measurements (see Ch. 2.3.1).

The water content of liquid particles will change according to the temperature and partial pressure of H_2O. As the temperature decreases, the particle absorbs water to maintain equilibrium, resulting in compositional change and particle growth. When the temperature rises, H_2O evaporates. The solubility of HNO_3 increases as the droplet becomes more dilute with H_2O. The particle thereby evolves into a liquid ternary solution droplet, PSC type 1b particle, with a composition depending on the partial pressure of both H_2O and HNO_3, as well as temperature. The liquid particles freeze instantaneously if the temperature falls below the ice frost point, near 188 K. If the temperature drops below 5 K above the ice frost point (the SAT-embryo temperature) and thereafter increases, SAT-embryo are assumed to form in the liquid particles. Subsequent cooling below the SAT-embryo temperature results in particle freezing. The HNO_3 present in the type 1b particles together with H_2O is deposited as NAT in a shell surrounding the solid H_2SO_4/H_2O core, resulting in PSC type 1a particles. The particles will then continue to grow as PSC 1a particles as the temperature drops further. The type 1a particles act as condensation nuclei for PSCs type 2 at temperatures below the ice frost point (Marti and Mauersberger, 1993). Hence, the model assumes that type 1 PSCs consist of a core of frozen sulphuric acid and a shell of NAT, whereas type 2 PSCs consist of a type 1a PSC core surrounded by a shell of crystalline ice.

When the temperature rises, the ice coating of the type 2 particles will evaporate, leaving type 1a particles. If the temperature increases further, the NAT will evaporate, leaving a SAT particle. The SAT particles melt and become liquid sulphuric acid particles above ~215 K. If the temperature drops again before the SAT particles have melted, the SAT particles act as condensation nuclei for PSC type 1a particles. Nitric acid vapour becomes supersaturated with respect to NAT at temperatures below roughly 193 K (Hanson and Mauersberger, 1988).

There are 50 size categories, or bins, in the model for which the size distribution for all the particle types is calculated. The particle radii range from 1 nm to 82.6 μm. The increase in size from one size bin to another is described by a geometrically increasing volume scale where the volume-ratio of adjacent bins is set equal to two. A specific bin holds the particles with radii spanned by the radius interval of that bin. As the particles grow or shrink they will be moved between the different size bins accordingly. The total surface area density ($\mu m^2 cm^{-3}$) of each particle type is calculated from the added sum of the number density of particles in each size bin. The microphysical calculations are performed with a time step of five minutes.

2.4 Calculation of chemical species

The chemistry scheme considers photodissociation, which is described in Ch. 2.2.2, reactions in the gas phase, and heterogeneous chemical reactions in the presence of particles. 58 chemical species made up of hydrogen, carbon, nitrogen, oxygen, chlorine and bromine are included in the model. This chapter gives a description of the numerical scheme, the gas phase and heterogeneous chemical reactions, the definition of ozone loss mechanisms and the determination of initial species concentration.

2.4.1 Numerical scheme

The numerical procedure used in this model is based on quasi-steady-state approximations (QSSA), and is described in Hesstvedt et al. (1978).

The change in concentration of a chemical species ($d[C]$) over a given time period (dt) is calculated from its initial concentration and the chemical production and loss over the time period, by means of the continuity equation (Hesstvedt et al., 1978).

$$\textit{Eq. 10} \qquad \frac{d[C]}{dt} = P - Q \cdot [C]$$

The species concentration, [C], is given in molec·cm^{-3}. The production term, P, is the number of molecules produced per second (molec·cm^{-3}·s^{-1}) over the time period, and is a sum based on all the chemical reactions leading to production. In the same way, the chemical loss, Q, is calculated from the reactions where the species is consumed. This quantity is given per second (s^{-1}). The concentration of a species at a time $t+\Delta t$ is calculated from its value at the previous time step, t, and its production and loss term by solving Eq. 10 analytically.

$$\textit{Eq. 11} \qquad [C]_{t+\Delta t} = \frac{P}{Q} + \left([C]_t - \frac{P}{Q} \right) \cdot e^{-Q\Delta t}$$

The terms P and Q are assumed to be constant over the time step, Δt. The chemical lifetime of a species, τ, is defined as the inverse of the loss term ($\tau = Q^{-1}$). The species are classified according to their lifetime relative to the time step, and one of three different solution methods is applied. In the photochemical trajectory model, the chemical integration time step is set to 15 minutes (900 s). At solar zenith angles between 86 and 96°, the time step is shortened to 90 s. The chemical lifetime of a species can vary considerably over the diurnal cycle and with season, latitude and longitude. It is therefore necessary to check the chemical lifetimes prior to each integration.

If the lifetime is short compared to the time step ($\tau < \Delta t/10$), the compound is assumed to be in equilibrium with the other species at any instant. In this case, the new concentration is computed from the production and loss terms, the so-called photochemical equilibrium value.

$$\textit{Eq. 12} \qquad [C]_{t+\Delta t} = \frac{P}{Q}$$

With a chemical time step of 15 minutes, photochemical equilibrium applies to species with a lifetime of less than 90 seconds. This criterion is applied also when the chemical time step is shortened at sunrise and sunset.

In the case where the lifetime is much longer than the time step ($\tau \gg \Delta t$), the variation in concentration is slow over the time period, and can be considered linear. The criteria used in the model is $\tau > 100\Delta t$. A time step of 15 minutes

results in a lifetime of approximately one day. In this case, the concentration is calculated by linear extrapolation.

Eq. 13 $[C]_{t+\Delta t} = [C]_t + \left(P - Q \cdot [C]_t \right) \cdot \Delta t$

The compounds with a lifetime comparable to the integration time step $(\Delta t/10 < \tau < 100\Delta t)$ are calculated from Eq. 11.

QSSA is a semi-analytical method, which excludes negative integration results, but does not preserve the number of atoms exactly. In order to alleviate this problem, related species are grouped into chemical families. The family approach is a means of avoiding uncontrolled growth or decline in any single component. The individual components within a family are scaled against the sum, thereby compensating for the possible artificial loss or gain of molecules in the integration.

The time step is basically chosen according to the lifetime of the shortest-lived species. By grouping species together in families, the time step can be lengthened. Members within a family will react rapidly with each other, but less efficiently with species from outside the family. The concentration of a family is calculated only on the basis of the reactions with species not included in the family, as the reactions between family members cancel out in the expression for the change in family concentration. The concentrations of the families and the individual species are calculated, after which the concentration of the individual species is adjusted relative to the family concentration.

The chemical families and all the species included in the model are defined in Table 1. The scheme includes 58 species, of which 18 are source gases. The concentrations of the species with a lifetime of one month or longer are not recalculated, but contribute to the production term of the other species. There are six chemical families, which are described shortly in the following.

Table 1:   Chemical species and families in the photochemical trajectory model.

Chemical families	Species in family
Odd oxygen (O_X)	$O(^3P) + O(^1D) + O_3$ - NO - Cl - Br
Odd hydrogen (HO_X)	$H + OH + HO_2 + 2\ H_2O_2$
Odd nitrogen (NO_Y)	$NO + NO_2 + NO_3 + 2\ N_2O_5 + HNO_2 + HO_2NO_2 + ClONO_2$
Odd chlorine (Cl_X)	$Cl + ClO + HOCl + ClONO_2 + 2\ Cl_2 + OClO + ClOO + 2\ Cl_2O_2 + HOOCl$
Reactive chlorine (Cl_Y)	$Cl_X + HCl(g)$
Reactive bromine (Br_Y)	$Br + BrO + HBr + BrONO_2 + HOBr + 2\ Br_2 + BrCl$
Source gases	N_2O, CH_4, CH_3Cl, $CHClF_2$, CCl_3F, CCl_2F_2, CCl_4, CH_3CCl_3, CH_3Br, $CBrClF_2$, $CBrF_3$, $C_2Br_2F_4$, $C_2Cl_3F_3$, $C_2Cl_2F_4$, C_2ClF_5, $CHCl_2CF_3$, CH_3CCl_2F, CH_3CClF_2
Other species	CO, CH_2O, CH_3O_2, CH_3OOH, H_2, H_2O, $H_2O(s)$, $HCl(s)$, $HNO_3(g)$, $HNO_3(s)$,

The sum of odd oxygen, O_X, is the added sum of O_3, $O(^3P)$ and $O(^1D)$ and the subtracted contribution of NO, Cl and Br. Production of O_X is therefore a result of the production of the first three members or a loss of the last three members. In the stratosphere, the dominant member of the family is O_3. The concentration of O_X and the individual concentrations of the other species are calculated and O_3 is retrieved by subtracting the concentrations of these species from O_X.

Odd hydrogen, HO_X, contains all hydrogen species except H_2, $H_2O(g)$ and $H_2O(s)$. The total mixing ratio of H_2O is 5 ppm, which is not altered through chemical reactions. The concentration of HO_X, the sum of H, OH and HO_2, and the individual species are calculated. The following scaling procedure does not affect the concentration of H, which is always in equilibrium with the other species. The largest of the species OH and HO_2 is set equal to the difference between the sum of H, OH and HO_2 and the individually calculated concentrations. The resulting concentrations of OH and HO_2 and that of H_2O_2 are scaled so that the sum of the members of the HO_X family equals the concentration of HO_X.

NO_Y includes all nitrogen species except $HNO_3(g)$ and $HNO_3(s)$, and its source gas, N_2O. The concentrations of NO_Y, $HNO_3(g)$ and $HNO_3(s)$ are closely coupled as the chemical loss and production term of each species are determined by the equivalent term of the other species. The individual members of the NO_Y family are calculated as follows. The species of highest concentration is set equal to the difference between the NO_Y concentration and the sum of the other species. The remaining species are set equal to their individually calculated concentrations. The concentration of $ClONO_2$ is then adjusted to the Cl_X family as described below, and all the NO_Y species are re-scaled according to the new concentration of $ClONO_2$.

The term Cl_X includes all chlorine species except HCl(g) and HCl(s) and its source gases. The total chlorine (Cl_Y) amount in the modelled air parcel is the sum of Cl_X and HCl(g). There is a similar close coupling between Cl_X, HCl(g) and HCl(s) as for NO_Y and HNO_3. The members of the Cl_X family are calculated individually, and the species concentrations scaled with the ratio between Cl_X and the sum of the species. The concentration of $ClONO_2$ is adjusted, if needed, to the concentration of NO_Y, after which the individual species in Cl_X are recalculated accordingly. An iteration is performed to ensure mass conservation in the Cl_X and NO_Y families.

The term Br_Y is the bromine equivalent of Cl_Y. The concentration of each species in Br_Y is calculated individually. The largest of the species $BrONO_2$, HBr, HOBr, BrCl and Br + BrO is set as the difference between the concentration of Br_Y and the sum of the rest of the species. The other species concentrations are set equal to their individually integrated values. If any of the species concentrations are negative, the partitioning is recalculated by scaling the concentration of the species with the ratio of Br_Y and the sum of the individual species. Finally, the concentrations of Br and BrO are calculated in the same way based on the sum of the two species. BrCl and $BrONO_2$ could have been included in the Cl_X and NO_Y families, respectively. However, they contribute very little to the overall concentration of these families, and their omission does not lead to any significant error.

2.4.2 Gas phase chemistry

The gas phase chemistry scheme is basically the same as the one used in the Oslo 2-D model (Stordal et al., 1985; Isaksen and Stordal, 1986; Stordal and Isaksen, 1987; Isaksen et al., 1990; Zerefos et al., 1997). It is developed to study stratospheric ozone and has been used in many assessment studies (e.g. Ko et al., 1995; Hofmann et al., 1999).

There are approximately 100 gas phase reactions implemented in the model, including unimolecular, bimolecular and trimolecular reactions. All the chemical gas phase reactions in the scheme are given in Table A.2 (temperature independent bimolecular reactions), Table A.3 (temperature dependent bimolecular reactions), Table A.4 (trimolecular reactions) and Table A.5 (unimolecular dissociation reactions) (see Appendix A). The rate coefficients are chosen in compliance with DeMore et al. (1997). The temperature independent gas phase reaction rate coefficients are set at the beginning of the trajectory run. The temperature dependent rate coefficients are calculated every time step in accordance with the changing temperature along the trajectory.

2.4.3 Heterogeneous chemistry

Heterogeneous reactions are assumed to take place in or on liquid particles and on the surface of solid particles. The particle types included in the model and the relationship between them are described in Ch. 2.3.2. Table 2 gives an overview of the heterogeneous chemical reactions that are implemented in the model, and the type of particles that facilitate them.

The reaction rate coefficients, k, for heterogeneous reactions taking place on the surface of particles are parameterised with reactive uptake coefficients (γ).

Eq. 14 $$k = \frac{\gamma \cdot S \cdot \bar{c}}{4}$$

Table 2: *Heterogeneous reactions implemented in the photochemical trajectory model and the particle types that facilitate them. The reactive uptake coefficients are listed in Table A.6 and Table A.7 (see Appendix A).*

Reaction		Reaction sites			
		liquid particles	SAT	NAT	ice
R 1	$ClONO_2 + H_2O \rightarrow HOCl + HNO_3$	x	x	x	x
R 2	$ClONO_2 + HCl \rightarrow ClNO_2 + HNO_3$	x	x	x	x
R 3	$HOCl + HCl \rightarrow Cl_2 + H_2O$	x		x	x
R 4	$N_2O_5 + H_2O \rightarrow 2\,HNO_3$	x	x	x	x
R 5	$N_2O_5 + HCl \rightarrow ClNO_2 + HNO_3$			x	x
R 6	$HOBr + HCl \rightarrow BrCl + H_2O$	x		x	x
R 7	$BrONO_2 + H_2O \rightarrow HOBr + HNO_3$	x		x	x
R 8	$BrONO_2 + HCl \rightarrow BrCl + HNO_3$	x			

18

The particle surface area density is denoted S, and $\bar{c}$ is the average relative molecular velocity. S for both liquid and solid particles is calculated by means of the microphysical model. The average molecular velocity is dependent on temperature and molecular mass (Turco et al., 1989), assuming that the mean free path of a molecule is greater than the particle radius. The mean value for the species in question under stratospheric conditions is $2 \cdot 10^{-4}$ cm·s^{-1}. The reactive uptake coefficients are chosen in accordance with the recommendations of DeMore et al. (1997) if not otherwise stated. The values are given in Table A.6 and Table A.7 (see Appendix A).

The rate coefficients for reaction on solid particles are parameterised according to Eq. 14. The solid particles are assumed to accommodate a monolayer of HCl(s) and the reaction rate of reactions R 2, R 3, R 5 and R 6 are calculated on the basis of the availability of HCl(s) at the surface of the particles.

Reaction R 4, R 7 and R 8 are assumed to take place on the surface of liquid sulphuric acid particles and are parameterised in the same way as for solid particles. The parameterisation of these reactions is therefore independent of temperature and particle composition. The reactions R 1 - R 3 and R 6 are assumed to take place in the bulk of the liquid particle. The reaction rate coefficient is dependent on the solubility of the reactants, which is determined by the weight percent of sulphuric acid (W% H_2SO_4). W% H_2SO_4 is calculated using an iterative procedure based on temperature and partial pressure of H_2O. Reactive uptake coefficients for reactions R 1 - R 3 and R 6 are based on laboratory measurements for bulk liquids at different temperatures and aerosol acidity. The reaction rate coefficients for R 2 and R 3 take into account the solubility of HCl in the aerosols, and the results are corrected for the small size of the aerosols in the stratosphere (Hanson et al., 1994). The rate coefficient of reaction R 6 is calculated from the liquid phase reaction rate (Danilin and McConnell, 1995). Figure 3 shows the calculated reactive uptake coefficients for reactions R 1 - R 3 and R 6 at different temperatures. The reactive uptake coefficient in a ternary solution at a given temperature is calculated by assuming a binary solution.
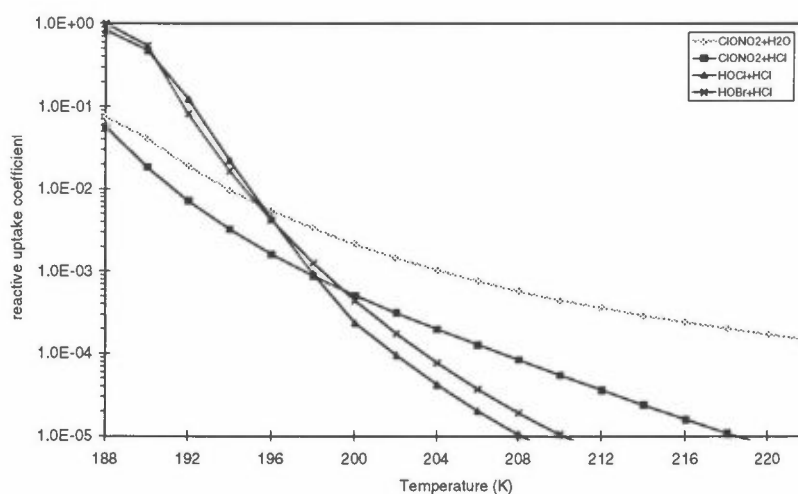

Figure 3: *Reactive uptake coefficients (γ) for heterogeneous reactions in liquid sulphuric acid particles as a function of temperature.*

2.4.4 Ozone loss mechanisms

There are a number of catalytic ozone loss cycles in the stratosphere. Individual reactions can be part of many different cycles and in order to quantify the contribution from the different cycles, reactions are grouped together in so-called loss mechanisms. This approach is useful for the interpretation of model results. The loss of odd oxygen is calculated from the rate-limiting step. The definition of loss mechanisms varies from model to model. The loss mechanisms defined in the photochemical trajectory model are the same as in the Oslo 2-D model (Stordal and Isaksen, 1987) and the reaction sequences are presented in Table 3.

Table 3:   Loss mechanism for odd oxygen parameterised in the photochemical trajectory model. The reactions referred to are listed in Appendix A.

Label	Short name	Reaction scheme	Loss of O_X
L 1	O_X	$O(^3P) + O_3 \rightarrow 2\ O_2$	-2
L 2	HO_X	$O_3 + OH \rightarrow HO_2 + O_2$ $O(^3P) + HO_2 \rightarrow OH + O_2$ $O_3 + OH \rightarrow HO_2 + O_2$ $O_3 + HO_2 \rightarrow OH + 2\ O_2$	-2 -2
L 3	NO_X	$O_3 + NO \rightarrow NO_2 + O_2$ $O(^3P) + NO_2 \rightarrow NO + O_2$	-2
L 4	$ClONO_2$	$ClONO_2 + h\nu \rightarrow Cl + NO_3$ $NO_3 + h\nu \rightarrow NO_2 + O$ $O_3 + Cl \rightarrow ClO + O_2$ $O_3 + NO \rightarrow NO_2 + O_2$ $NO_2 + ClO + M \rightarrow ClONO_2 + M$	-1
L 5	ClO_X	$O_3 + Cl \rightarrow ClO + O_2$ $O(^3P) + ClO \rightarrow Cl + O_2$	-2
L 6	BrO+ClO	$BrO + ClO \rightarrow Br + ClOO$ $ClOO + M \rightarrow Cl + O_2 + M$ $BrO + ClO \rightarrow BrCl + O_2$ $BrCl + h\nu \rightarrow Br + Cl$ $2(O_3 + Cl \rightarrow ClO + O_2)$ $2(O_3 + Br \rightarrow BrO + O_2)$	-4
L 7	ClOOCl	$Cl_2O_2 + h\nu \rightarrow ClOO + Cl$ $ClOO + M \rightarrow Cl + O_2 + M$ $2(O_3 + Cl \rightarrow ClO + O_2)$ $ClO + ClO + M \rightarrow Cl_2O_2 + M$	-2
L 8	HOCl	$HOCl + h\nu \rightarrow OH + Cl$ $O_3 + OH \rightarrow HO_2 + O_2$ $O_3 + Cl \rightarrow ClO + O_2$ $HO_2 + ClO \rightarrow HOCl + O_2$	-2
L 9	HOBr	$HOBr + h\nu \rightarrow OH + Br$ $O_3 + OH \rightarrow HO_2 + O_2$ $O_3 + Br \rightarrow BrO + O_2$ $HO_2 + BrO \rightarrow HOBr + O_2$	-2

2.4.5 Initialisation of chemical species

The initial concentrations of chemical species and total air number density (M) are taken from a two-dimensional climatological model (The Oslo 2-D model, Stordal et al., 1985). The results from the 2-D model are stored in a latitude and altitude grid for the last day of the month. The latitudinal resolution is $10°$ and the horizontal resolution is 2 kilometres.

The initial values for the photochemical trajectory model are obtained through interpolation between the nearest grid points in the 2-D model. The trajectory model uses a pressure and temperature co-ordinate system, while the input data are given at fixed altitudes. Based on the temperature and total air number density, the pressure of the height levels in the 2-D model is calculated according to the hydrostatic equation. The input values for the trajectory model are obtained through logarithmic interpolation between the appropriate altitude levels and linear interpolation with respect to latitude. The initial chemical species concentrations from the 2-D model are chosen for the appropriate month.

The 2-D model is run with different scenarios and under different conditions. The data represent monthly and latitudinal means, and do not, therefore, reflect the latitudinal variations in chemical tracer fields, or the day-to-day variation. The photochemical model is initialised with noon values. The results from the photochemical trajectory model are sensitive to the initial values, because there is no exchange with the surrounding air during the calculations. Thus, the initial concentration of Cl_Y, NO_Y, HO_X and Br_Y governs the potential for active species concentrations. The partitioning of species over the calculation period is determined by the evolution of temperature and solar radiation.

2.5 Air parcel trajectories

The winds in the atmosphere vary both in magnitude and direction according to pressure and temperature. The movements of air parcels can be described by air parcel trajectories calculated on the basis of observed meteorological parameters. The photochemical trajectory model requires data on horizontal movement (latitude and longitude), temperature and either ambient or surface pressure or geopotential height. So far only isentropic trajectories have been used.

The calculations of the realistic air parcel trajectories used in connection with the photochemical model are described in the first subsection. In the present study, the model is used as a box model, and calculations are made at fixed latitudinal and altitudinal positions. The in-situ chemical evolution can thus be studied dependent only on temperature and diurnal variation of solar radiation. The second subsection describes the calculation of temperatures for a given month, latitude and height.

2.5.1 Calculation of air parcel trajectories

A model developed at the Danish Meteorological Institute (Knudsen and Carver, 1994) has been used during several European campaigns (European Commission, 1997). The trajectory model uses realistic meteorological data, based on initialised analysis data from the European Centre for Medium-Range Weather Forecasts (ECMWF). The model provides data for position (latitude and longitude), temperature, surface pressure and potential vorticity (PV). 10-day trajectories are

calculated for a number of arrival sites in the Northern Hemisphere. The trajectories are calculated backward from the arrival point. The two-dimensional trajectories for isentropic levels corresponding to the potential temperatures 350, 380, 400, 435, 475, 550 and 675 or 700 Kelvin (K) are calculated every day during the winter season. The isentropic nature of the trajectories assumes that the potential temperature (θ) is constant throughout the 10-day period. The trajectories are calculated with a time step of 15 minutes and data are stored every 2 hours. The fields are interpolated linearly in space on a 1.5° by 1.5° latitude-longitude grid, and in time between the 6 hourly analysis provided by ECMWF. There are 31 vertical pressure levels. For the 1991/92 to 1997/98 winters, backward trajectories have been calculated for most sites where measurements are carried out. In addition, trajectories ending at 118 grid points covering the Northern Hemisphere north of 30°N in an equal area grid have been calculated from 1993/94.

2.5.2 Stationary air parcels

Monthly mean temperatures for certain latitudes and isentropic levels have been calculated, based on ECMWF temperatures from 1997 in a 1.125° by 1.125° grid. The daily average temperature and standard deviation (σ) for each latitude band and height have been calculated, and based on these values, a monthly mean
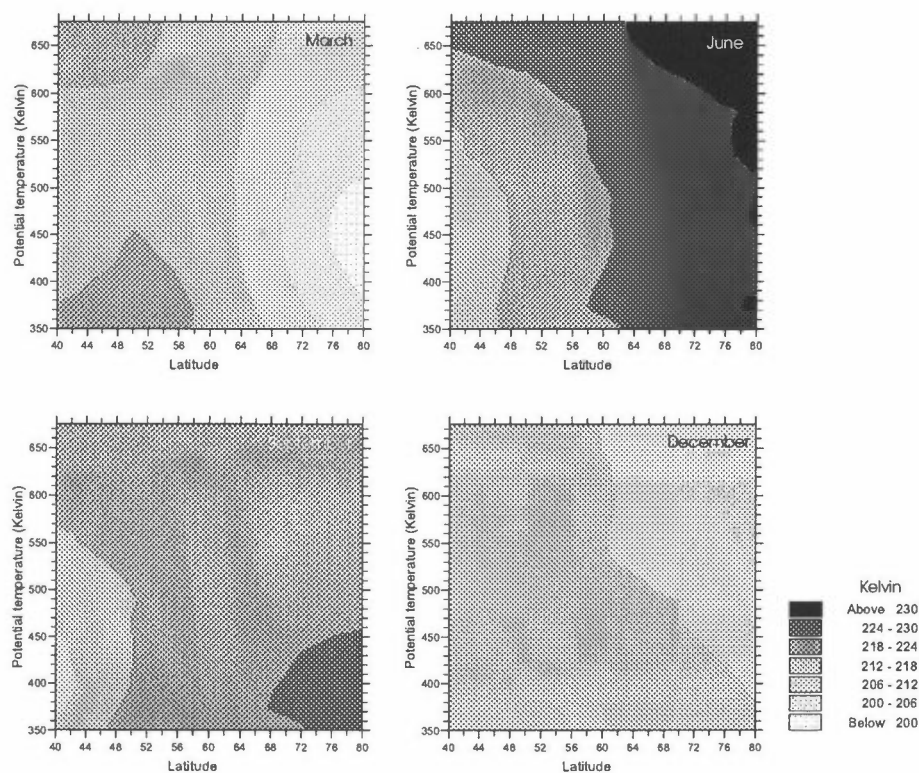

Figure 4:   Mean monthly temperatures from 1997 for the latitudes 40, 50, 60, 70 and 80°N and the isentropic surfaces 350, 380, 400, 435, 475, 550 and 675 K, calculated from ECMWF data. The mean temperatures for March (upper left panel), June (upper right panel), September (lower left panel) and December (lower right panel) are shown.

temperature and standard deviation is calculated for each month, latitude band and height level. The resulting standard deviation expresses the deviation from the mean temperature over a latitude band in the course of one month. Calculations have been made for the latitudes 40, 50, 60, 70 and 80°N at the potential temperature surfaces 350, 380, 400, 435, 475, 550 and 675 K. Monthly mean temperatures for the months January through April, and for June, September and December have been calculated. The mean temperatures have been used in the calculations presented in this study and the values are given in Appendix B. Figure 4 shows the monthly mean temperature at each latitude and isentropic level for March, June, September and December 1997.

2.6 Model output

The results from the photochemical trajectory model are stored in the form of chemical species concentrations, particle surface area densities and various meteorological, physical and chemical parameters. The net loss of ozone (D_{O_3}) is derived from the ozone mixing ratio at the start of the calculations subtracted from the mixing ratio at end of the integration. D_{O_3} is given in ppb·day^{-1}. Since there is no transport of air included in the calculations, the overall change in ozone concentration is a result of the balance between production (P_{O_3}) and loss ($Q_{O_3} \cdot C_{O_3}$) (Eq. 10). The chemical lifetime of ozone, τ_{O_3}, is defined as $1/Q_{O_3}$. Ozone is lost chemically through a number of different mechanisms. The relative importance of the different loss mechanisms depends on solar radiation, the concentration of species and the chemical processes included in the reaction scheme. The loss mechanisms defined in this model are listed in Table 3 (Ch. 2.4.4). The ozone loss rate is given as average loss per day over the integration period (molec·cm^{-3}·day^{-1}).

The results of the model calculations reflect the evolution only at a defined height interval. In order to obtain a spatial image, the results can be interpolated between the isentropic levels and latitudes. To obtain results for a height region, the data for several height levels can be integrated and added up. The integration is done in pressure segments, and the column will cover approximately 10 to 27 kilometres, depending on latitude and season.

3. Results and discussion

Chemical box model calculations were made over a month at 35 locations at middle to high latitudes on seven isentropic surfaces. The latitudes range from 40 to 80°N, at 10° intervals. The isentropic surfaces used in this study are 350, 380, 400, 435, 475, 550 and 675 K. Monthly mean temperatures (see Ch. 2.5.2) for a given latitude and isentropic surface were used in the calculations. The model calculations do not include the effect of transport and the results reflect only the chemical conversion of species through chemical production and loss processes, as there is no exchange of matter with the surrounding air. Only liquid sulphuric acid aerosols were included as reaction sites for heterogeneous reactions. The formation of liquid ternary particles through uptake of nitric acid has been suppressed, although the temperature range used indicates that such particles would form. Two scenarios for aerosol surface area densities based on satellite observations have been taken into account. Observations from 1979 have been used as background conditions and data from 1992 as representative for volcanic

conditions (see Ch. 2.3.1). The initial chemical species concentrations used in this study are taken from a 2-D model simulation including gas phase chemistry and heterogeneous reactions on background sulphuric acid particles, without activation on PSC particles. Values for the year 1994 are used. Each monthly integration was initialised with 2-D output data.

Calculations including only gas phase reactions are presented in Ch. 3.1. These calculations are presented in order to access the impact of the heterogeneous reactions presented in later sections. Heterogeneous chemical reactions assumed to take place in connection with stratospheric sulphate particles are given in Ch. 2.4.3. These reactions have been implemented in the photochemical trajectory model, and the results are presented in Ch. 3.2. In addition, some reactions proposed within the LAMOCS project have been implemented. These results are presented in Ch. 3.3.

3.1 Gas phase chemical reactions

Model calculations including only gas phase chemical reactions have been made for the months of March (spring equinox), June (summer solstice), September (autumn equinox) and December (winter solstice) representing the four seasons. In addition, calculations have been made for January, February and April. The results from the latter set are not presented here, but are used to assess the impact of heterogeneous self-activation of chlorine in Ch. 3.3.1.

Both the loss (Q_{O_3}) and production (P_{O_3}) of ozone varies with photochemical activity, which is dependent on the intensity of solar radiation. The calculated mean net loss of ozone (D_{O_3}) therefore varies greatly in magnitude with latitude, altitude and season. The magnitude of the overall loss rates is reflected in the chemical lifetime of ozone (τ_{O_3}). Figure 5 shows the calculated mean chemical lifetime of ozone for 40-80°N and 350-675 K for March and June. τ_{O_3} generally decreases with altitude at a given latitude. The lifetimes calculated for September (not shown) exhibit a similar pattern as for March, but are generally shorter at a given height. In December (not shown), the intensity of solar radiation decreases with latitude, leading to an increase in the chemical lifetime of ozone. At the northernmost latitudes, there is effectively no chemical activity at this time of year.
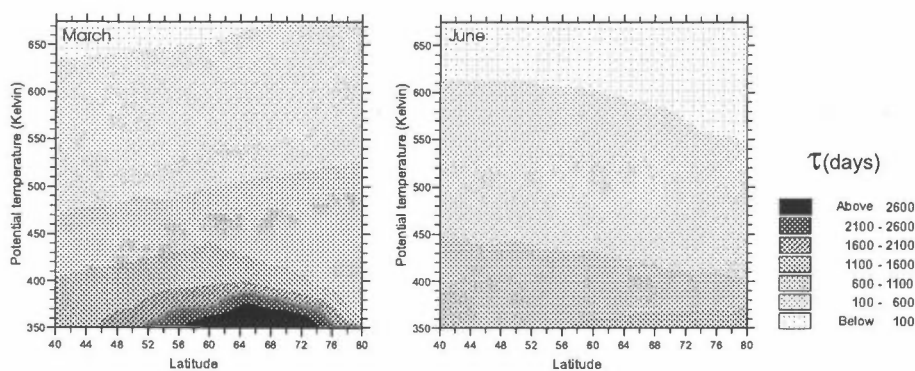

Figure 5: Monthly mean chemical lifetime of ozone (τ_{O_3}) in days, calculated at 40-80°N and 350-675 K for the months of March (left panel) and June (right panel). The simulations include only gas phase chemistry.
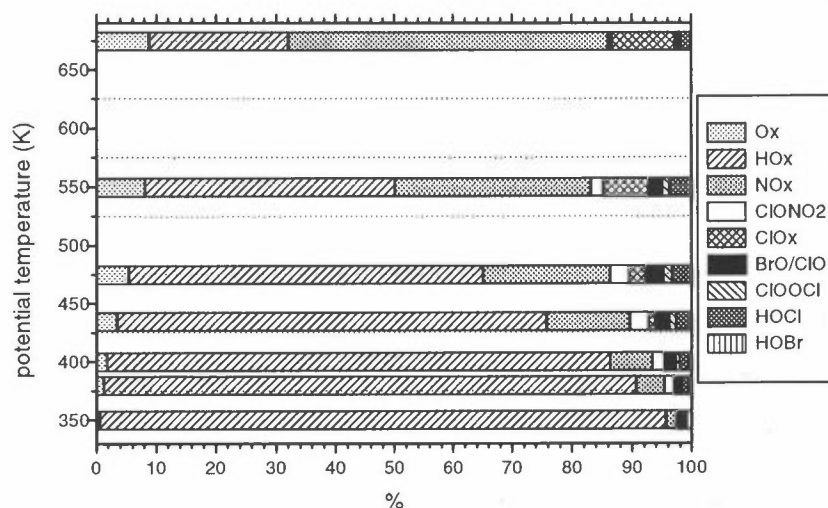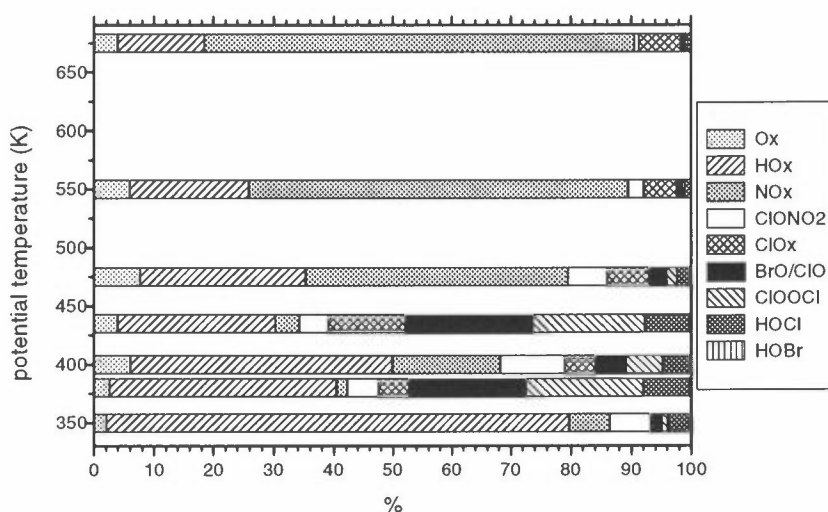
Figure 6: The contribution from the different ozone loss mechanisms (%) at 40°N in March for the gas phase reaction scheme.

Figure 6 shows the percentage contribution from the different ozone loss mechanism at 40°N in March, which is representative of most latitudes and seasons. The ozone loss at 675 K is dominated by the catalytic NO_X cycle (L 3). The second most important loss mechanism is the catalytic HO_X cycles (L 2). The only other significant loss mechanisms are the catalytic ClO_X cycle (L 5) and the reaction within the O_X family (L 1). At decreasing altitude, the overall ozone loss rates decrease (seen as an increase in chemical lifetime in Figure 5), while the catalytic HO_X cycles (L 2) account for an increasing fraction of the ozone loss. The quantitative and relative importance of the catalytic NO_X cycle (L 3) increases with latitude (Figure 6 versus Figure 7).

The exceptions to this general picture are found at high latitudes (70 and 80°N) in March. In this case, the ozone loss rates decline below 475 K (seen as a decrease

Figure 7: The contribution from the different ozone loss mechanisms (%) at 70°N in March for the gas phase reaction scheme.

in chemical lifetime in Figure 5). This is a result of the initial species concentrations, reflecting the Brewer-Dobson circulation with downward transport in the lower stratosphere at high latitudes. The quantitative contribution from the chlorine and bromine cycle (L 6) and the ClO-dimer cycle (L 7) is much larger in this region. This can be seen in Figure 7, which shows the relative contribution of the different ozone loss mechanisms at 70°N in March at all seven isentropic surfaces.

In the upper part of the studied altitude region, the catalytic NO_X cycle is the dominant ozone loss cycle at high latitudes in spring, in quantitative agreement with the 2-D model calculations presented by Perliski et al. (1989). In June, the NO_X cycle account for 60 to 70% of the chemical ozone destruction at high latitudes above 475 K. This is in good agreement with the box model calculations performed by Brühl et al. (1998) which indicate 70%.

Figure 8 shows the calculated net ozone loss (D_{O_3}). The highest net loss is calculated at 80°N on the 675 K isentropic surface for March (17 ppb·day^{-1}), June (20 ppb·day^{-1}) and September (25 ppb·day^{-1}). At all other latitudes in March, the highest net loss is calculated at 550 K. The overall net loss is to a large degree controlled by the rate of ozone production, which increases with decreasing latitude. At low latitudes, the model calculates a production of ozone at the top and the bottom of the altitude region for all three months. In December, the maximum loss is calculated at middle latitudes on the 675 K level (~24 ppb·day^{-1}).
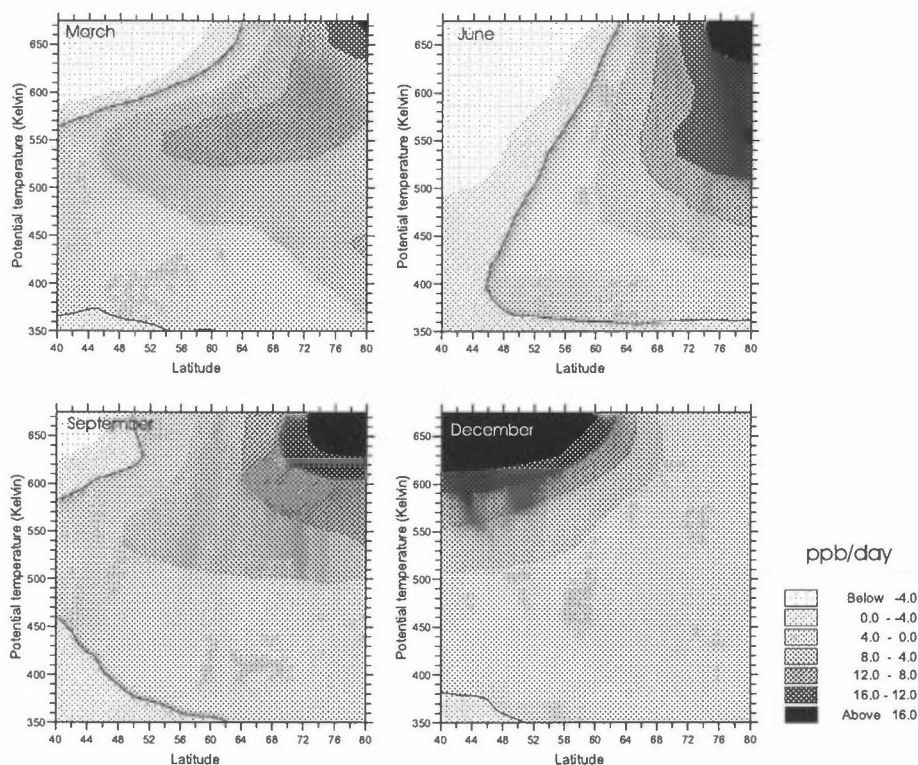

Figure 8: Monthly mean net ozone loss (D_{O_3}) calculated for stationary air parcels at 40-80°N and 350-675 K. The thin line indicates the division of the modelled production or loss of ozone. Calculations including only gas phase chemistry have been made for March (upper left panel), June (upper right panel), September (lower left panel) and December (lower right panel). The results are given in ppb·day^{-1}.

3.2 The impact of established heterogeneous reactions

In the first section, the impact of heterogeneous nitrogen and chlorine reactions (R 1–R 4) relative to a scenario with only gas phase chemistry is quantified. The second section focuses on heterogeneous bromine reactions (R 6-R 8). Calculations including heterogeneous bromine reactions, with or without chlorine and nitrogen reactions are compared to those of the previous section, and the importance of the different ozone loss cycles is quantified. The time evolutions of some key species are presented for the different reaction schemes in the third section. The in-situ chemical ozone reduction in the lower stratospheric column abundance is presented in the fourth section.

3.2.1 Chlorine and nitrogen reactions

The occurrence of the heterogeneous reactions R 1–R 4 in connection with liquid sulphuric acid aerosols is well-established (Jones et al., 1995). Calculations including gas phase chemistry and heterogeneous reactions R 1–R 4 have been made for the same months as in Ch. 3.1. Simulations have been performed for scenarios with background and volcanically enhanced liquid particles. In the following, the results are discussed in relation to those obtained with the gas phase only reaction scheme presented in the previous section.

The introduction of heterogeneous reactions has the greatest impact in the region with highest aerosol loading (see Figure 1), and is in some cases enhanced by cold temperatures (see Figure 4). The reactive uptake coefficients for the reactions that activate chlorine directly (R 1-R 3) are temperature dependent (see Figure 3). The activation rate through these reactions is therefore dependent on the spatial distribution of temperature, aerosol surface area density and concentration of reactants. The reactive uptake coefficient for the N_2O_5 hydrolysis reaction (R 4) is temperature independent, and the reaction rate coefficient therefore varies only with the aerosol surface area density and concentration of reactants.

The conversion of N_2O_5 to HNO_3 (R 4) and subsequent photolysis results in higher concentrations of OH, but lower concentrations of NO_2 compared to the gas phase run, because the photodissociation coefficient for HNO_3 is lower than that of N_2O_5. The ozone loss through the catalytic HO_X cycles (L 2) is thereby enhanced while the importance of the catalytic NO_X cycle (L 3) is reduced. Further, the additional HO_X results in additional chlorine activation through the reaction between OH and HCl. The concentration of HOCl and $ClONO_2$ is enhanced due to the subsequent increase in the concentration of ClO. The net effect of the N_2O_5 hydrolysis reaction on the ozone concentration depends on the magnitude of the reduced loss through L 3 compared to the added loss through L 2. This balance is determined by the heterogeneous reaction rate and the photolysis rate of HNO_3.

At sufficiently low temperatures (at high latitudes in winter), chlorine is activated directly through reactions R 1-R 3 followed by photolysis of the reaction products, converting $ClONO_2$, HCl and HOCl to Cl and ClO. This directly enhances the ClO-dimer loss mechanism (L 7), the chlorine and bromine loss mechanism (L 6) and the catalytic ClO_X cycle (L 5). ClO reacts with HO_2 to form HOCl and the HOCl photolysis mechanism (L 8) is thereby enhanced. Figure 9 shows the quantitative differences in ozone loss mechanisms at 70°N in March by
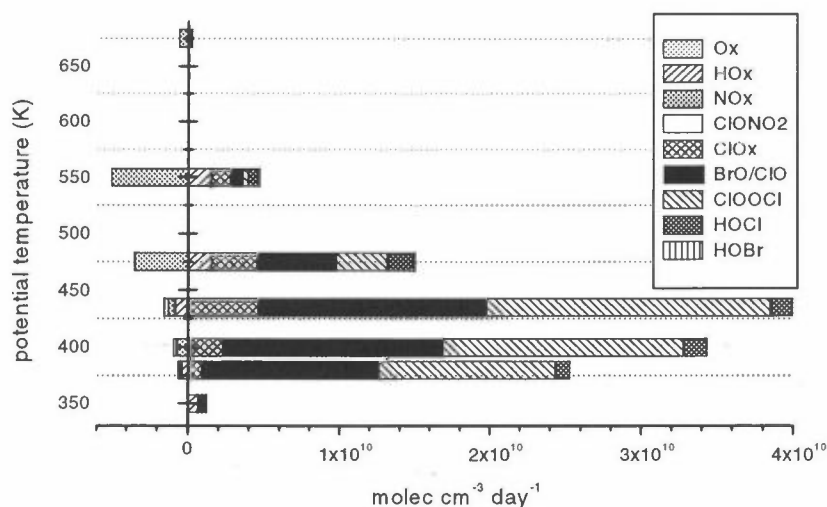
Figure 9: *The difference in ozone loss rates (molec·cm⁻³·day⁻¹) for the different loss mechanisms at 70°N in March by adding heterogeneous chlorine and nitrogen reactions (R 1–R 4) on volcanic aerosols to the gas phase reaction scheme.*

adding heterogeneous reactions R 1–R 4 on volcanic aerosols compared to the gas phase scheme shown in Figure 7. The effect of background particles is qualitatively the same as for volcanic aerosols, but the quantitative contribution is much smaller.

Figure 10 shows the difference in net ozone loss (D_{O_3}) for March by adding the heterogeneous chlorine and nitrogen reactions (R 1–R 4) on background and volcanically enhanced liquid particles to the gas phase reaction scheme shown in Figure 8 (upper left panel). At middle latitudes, the introduction of heterogeneous reactions on volcanic particles in March results in the largest additional net ozone loss at 550 K (~6 ppb·day⁻¹). The temperatures are too high for direct heterogeneous chlorine activation to take place. However, the photochemical activity is high at these latitudes, and the ozone loss is therefore increased mainly as a result of the N_2O_5 hydrolysis and subsequent enhancement of the catalytic HO_X cycles (L 2) and indirect chlorine activation, as described above.

In the upper part of the altitude region, the N_2O_5 hydrolysis reaction results in a reduction in the net ozone loss and subsequent enhancement of the ozone concentration in certain regions compared to the gas phase run (see Figure 10). This is due to the reduction in the NO_X loss cycle (L 3) which is not compensated by the increase in HO_X (L 2) and chlorine loss cycles (see Figure 9).

For the volcanic scenario, the largest additional net ozone loss is calculated at 70°N, 435 K (14 ppb·day⁻¹) and 80°N, 400 K (20 ppb·day⁻¹) as a result of chlorine activation through reaction R 1-R 3 and the subsequent effects described above (see also Figure 9). This additional loss results in the highest total net ozone loss for the volcanic case in March (not shown) amounting to 18 ppb·day⁻¹ at 70°N, 435 K and 26 ppb·day⁻¹ at 80°N, 400 K.
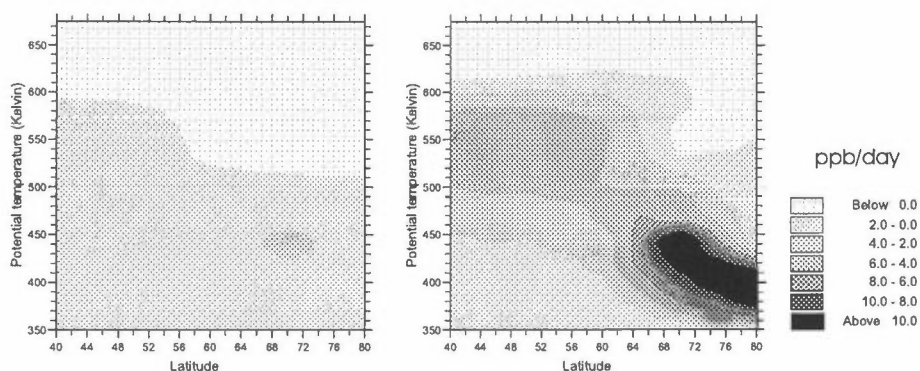
Figure 10: Difference in net ozone loss (D_{O_3}) by adding heterogeneous reactions R 1-R 4 to the gas phase run shown in Figure 8. Calculations for March with background aerosols (left panel) and volcanic aerosols (right panel) are shown.

In June, September and December the heterogeneous reactions that activate chlorine directly do not have any substantial effect. This is because the occurrence of high aerosol area, sufficiently cold temperatures and sunlight to drive the photochemical destruction cycles seldom coincide. In the cases where the ozone loss is enhanced, this is due to the effects of the N_2O_5 hydrolysis. The effect is most pronounced at 40°N, 550 K for all three months, and is of the same magnitude as in March. At high latitudes in June, there is continuous sunlight, resulting in N_2O_5 photolysis and subsequent reduction in heterogeneous conversion of N_2O_5.

The qualitative effect of adding reactions R 1-R 4 on background particles is the same as in the volcanic case. The quantitative effect is considerably reduced due to the lower heterogeneous reaction rate coefficients, and the added net ozone loss is less than 3 ppb·day^{-1} at all locations during all seasons.

The monthly ozone column loss between 350 and 675 K has been calculated. The difference between the resulting column ozone loss for the simulation with the gas phase reactions and that including heterogeneous reactions (R 1–R 4) on volcanic aerosols is presented in Table 4. The results are presented in Dobson units (DU) for all four months and five latitudes.

The addition of reactions R 1-R 4 results in the largest additional depletion of column ozone at high latitudes in March. This is because of the efficiency of the temperature dependent heterogeneous chlorine reactions. The added loss amounts to ~20 DU, which is a an additional 5% loss in column ozone. At middle latitudes, the calculated added reduction in column ozone for all seasons is 2-8 DU (see Table 4), corresponding to an increase of 1-2.5%.

For the background scenario, the reduction in column ozone is ~3 DU at high latitudes in March. The added loss for other seasons at high latitudes, and for all seasons at middle latitudes, is insignificant (≤1 DU).

Table 4: *Difference in column ozone (DU) after 30 days of integration between 350 and 675 K by adding heterogeneous reactions R 1-R 4 on volcanic aerosols to the gas phase reaction scheme.*

Latitude	40°N	50°N	60°N	70°N	80°N
March	-5.8	-7.8	-8.9	-21.8	-20.1
June	-5.1	-6.5	-5.7	2.3	1.1
September	-4.7	-5.4	-6.0	-5.1	0.6
December	-3.1	-2.3	-1.9	-0.5	0.0

3.2.2 Bromine reactions

Calculations including the heterogeneous bromine reactions R 6-R 8 on volcanic aerosols have been made with and without heterogeneous chlorine and nitrogen reactions (R 1-R 4). The results are compared to those presented in Chs. 3.1 and 3.2.1.

The reaction rate coefficients of reactions R 7 and R 8 are temperature independent and the efficiency of these reactions is only affected by the spatial distribution of aerosols and reactants. R 6 is sensitive to temperature but the reaction rate coefficient of this reaction is low at temperatures above ~200 K (see Figure 3). The impact of adding only reaction R 6 to the reaction scheme is therefore negligible at all latitudes and seasons since the mean temperatures used in this study are higher than 200 K, except at very high altitudes in March (see Figure 4).

Reaction R 7 and R 8 convert odd nitrogen into HNO_3 and activate the night time reservoir $BrONO_2$. HOBr produced through reaction R 7 either photolyses or reacts with HCl (R 6) to form BrCl. The reaction between $BrONO_2$ and HCl (R 8) directly activates chlorine by formation of BrCl, which easily photolyses, leading to an increase in the ClO and BrO concentrations. The effect of the formation of HNO_3 and subsequent photolysis results in indirect activation of chlorine, reduction of NO_2 and enhancement of HO_X as described in the previous section. The concentration of BrO is enhanced compared to the gas phase run due to the conversion of NO_X to HNO_3 and the subsequent suppression of $BrONO_2$ formation. The increase of ClO leads to enhanced levels of $ClONO_2$ relative to the scenario without heterogeneous bromine reactions. In the areas with high particle loading, the reaction rate coefficients of reactions R 7 and R 8 become very high. The chlorine is therefore in some cases completely activated.

The added reactions cause an enhancement in the chlorine and bromine mechanism (L 6), the ClO-dimer cycle (L 7), the catalytic chlorine cycle (L 5) and HOCl photolysis cycle (L 8) in the height region with high particle concentration. Figure 11 shows the quantitative difference in loss cycles for ozone at 70°N in March by adding the heterogeneous bromine reactions on volcanic aerosols to the heterogeneous chlorine and nitrogen reactions. All the loss cycles involving halogen species peak at 380-475 K. The dominating loss cycle for ozone involving halogen species is the ClO-dimer cycle (L 7) followed by active bromine reacting with active chlorine (L 6). The loss of ozone through the
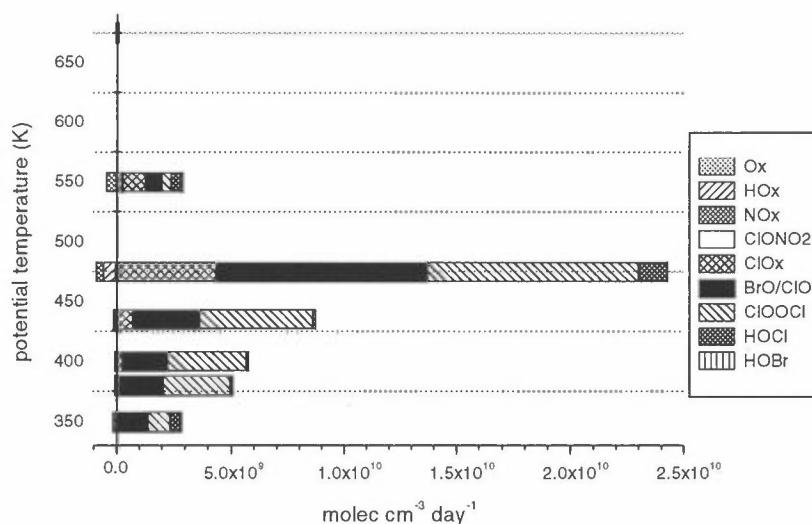
Figure 11: *The difference in ozone loss rates (molec·cm⁻³·day⁻¹) for the different loss mechanisms at 70°N in March by adding heterogeneous bromine reactions (R 6-R 8) on volcanic aerosols to the reaction scheme with gas phase reactions and heterogeneous chlorine and nitrogen reactions (R 1-R 4).*

catalytic HO_X cycles (L 2) has its maximum at 550 K. The catalytic NO_X cycle (L 3) becomes important at 675 K (~25 km).

Figure 12 shows the difference in net ozone loss calculated in March and June, by adding the heterogeneous bromine reactions on volcanic particles to the gas phase chemistry scheme (upper panels) and to the heterogeneous chlorine and nitrogen reaction scheme (lower panels) presented in Chs. 3.1 and 3.2.1, respectively. The effect of the heterogeneous bromine reactions is a result of coinciding high concentrations of bromine and large aerosol surface area density. The concentration of total inorganic bromine generally increases with latitude. The impact of the added reactions is most pronounced at high latitudes in the scenario including heterogeneous chlorine and nitrogen reactions because the loss cycle involving active bromine also includes active chlorine (L 6) (see Figure 12).

The most pronounced effect of the bromine reactions in March is calculated at 60 and 70°N, 475 K leading to an additional net ozone loss of 5 to 11 ppb·day⁻¹. At middle latitudes, the effect is most pronounced at 550 K, amounting to an additional loss of ~6 ppb·day⁻¹.

In June, the heterogeneous bromine reactions cause a substantial enhancement in depletion rates at 475 K at high latitudes. The additional loss in June is 23 ppb·day⁻¹ at both 70 and 80°N when heterogeneous chlorine reactions are included. This results in a total net loss of ~31 ppb·day⁻¹ in this region, which is the highest in June. In the scenario without heterogeneous chlorine reactions, the maximum additional loss is at 70°N, 475 K (10 ppb·day⁻¹). The high additional loss is caused mainly by the reaction between $BrONO_2$ and HCl (R 8) which

activates chlorine directly when no other pathways for heterogeneous activation of chlorine are active.

The ozone column concentrations between 350 and 675 K have been calculated and the monthly mean reduction in ozone as a result of adding heterogeneous bromine reactions to the simulation with heterogeneous chlorine and nitrogen reactions on volcanic aerosols is given in Table 5.

The effect of adding heterogeneous bromine reactions on background particles is less than 3 DU at all latitudes in all seasons. The addition of heterogeneous bromine reactions on volcanic particles at middle latitudes results in an additional in-situ reduction in column ozone of 4 to 16 DU per month, corresponding to 1.5-4 %. The highest loss is calculated for June and the lowest for December at all latitudes. At high latitudes, the greatest effect is calculated in June. The additional column loss is 30 to 53 DU, corresponding to 9-16 %.
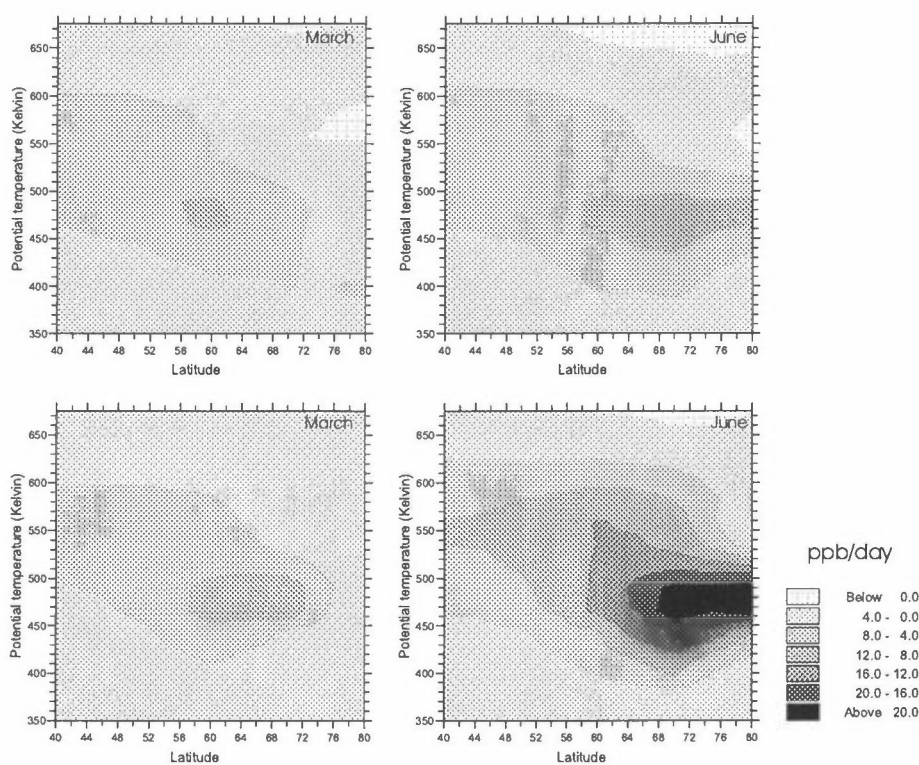
Figure 12: Difference in net ozone loss by adding heterogeneous bromine reactions (R 6-R 8) on volcanic aerosols to the gas phase reaction scheme shown in Figure 8 (upper panels) and in addition, heterogeneous chlorine and nitrogen reactions (R 1-R 4) (lower panels). Results for March (left panels) and June (right panels) are shown.

Table 5:   *Difference in mean monthly column ozone depletion (DU) between 350 and 675 K by adding heterogeneous bromine reactions (R 6-R 8) to the heterogeneous chlorine and nitrogen reactions (R 1-R 4) on volcanic aerosols.*

Latitude	40°N	50°N	60°N	70°N	80°N
March	-7.7	-11.0	-19.0	-11.7	-1.0
June	-10.3	-16.4	-31.5	-52.6	-28.7
September	-6.3	-7.5	-10.9	-16.1	-18.2
December	-3.5	-4.1	-4.7	-0.1	0.0

3.2.3 Time evolution of species

The step by step addition of heterogeneous reactions affects the partitioning within several of the compound families. Figure 13 shows how the mixing ratios of HCl, HNO_3 and O_3 evolve during March at 70°N and 475 K, for three different reaction schemes on volcanic aerosol as calculated by the photochemical trajectory model. Figure 14 shows the diurnal variation of OH, NO_2, ClO, $ClONO_2$, BrO, $BrONO_2$ for the last day of the one month integration period. The three reaction schemes are gas phase chemistry only (see Ch. 3.1), heterogeneous chlorine and nitrogen reactions (R 1–R 4) on volcanic aerosols (see Ch. 3.2.1), and all the heterogeneous reactions (R 1–R 4 and R 6–R 8) on volcanic aerosols (see Ch. 3.2.2). The general trends are the same for all latitudes and heights, although there are quantitative differences due to the spatial distribution of the different species.
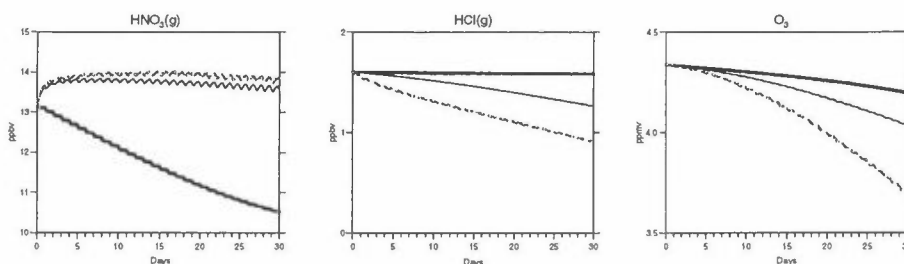

Figure 13:   *Mixing ratios for HNO_3, HCl and ozone in March at 475 K using volcanic aerosols. The thick solid line shows the gas phase reaction scheme, the thin solid line includes reactions R 1-R 4, and the dashed line is with all reactions (R 1-R 4 and R 6-R 8).*

In the gas phase case, HNO_3 is lost mainly through photodissociation to NO_2 and OH. HNO_3 is produced through the heterogeneous reactions, maintaining the level of HNO_3 to a varying degree at the expense of the odd nitrogen compounds. The NO_2 mixing ratio is highest in the gas phase case and is lowered as more efficient heterogeneous reaction schemes are added, due to the reduction of N_2O_5 and the reaction with active chlorine.
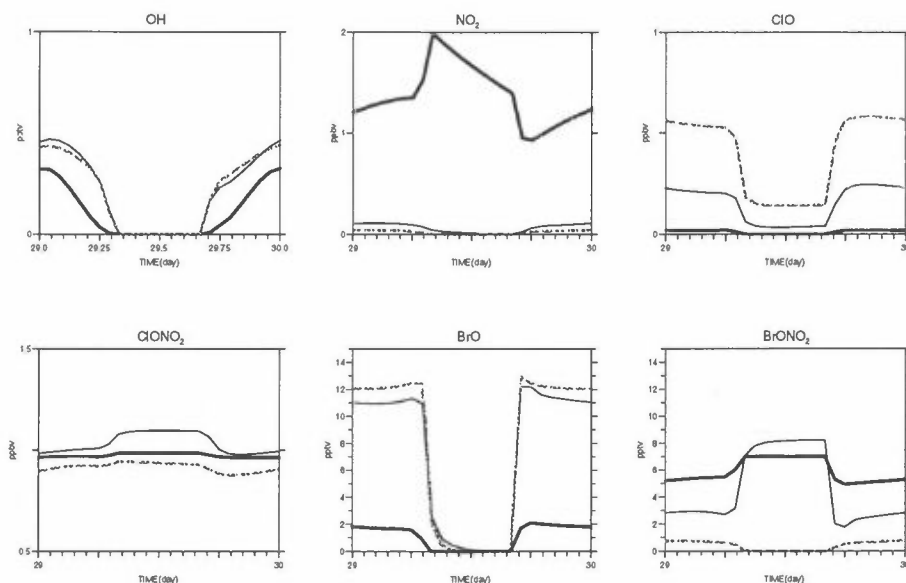
Figure 14: Mixing ratios for OH, NO$_2$, ClO, ClONO$_2$, BrO, BrONO$_2$ for the last day of the one month integration period shown in Figure 13. The thick solid line shows the gas phase reaction scheme, the thin solid line includes reactions R 1-R 4, and the dashed line is with all reactions (R 1-R 4 and R 6-R 8).

The concentration of inactive chlorine, in the form of HCl, is reduced through heterogeneous activation. The reduction is increased with the efficiency of the heterogeneous reaction scheme. The activation of chlorine can be seen in the elevated levels of ClO. In the case with heterogeneous bromine reactions, the level of ClONO$_2$ is reduced, as the availability of NO$_2$ limits the formation of ClONO$_2$.

BrONO$_2$ acts as a night-time reservoir for bromine. When heterogeneous bromine reactions are added, BrONO$_2$ is reduced during the night-time through the efficient heterogeneous reaction with H$_2$O and HCl on sulphuric acid aerosols. The BrO concentration increases as a response to the BrONO$_2$ reduction.

3.2.4 In-situ chemical loss of column ozone

The in-situ reduction in column ozone in the lower stratosphere between the 350 and 675 K isentropic surfaces has been calculated. Because most of the ozone resides in this height region, the calculated change is a good indicator of in-situ chemical loss of column ozone. The calculations include gas phase reactions and heterogeneous chlorine, bromine and nitrogen reactions taking place in connection with background or volcanically enhanced liquid sulphuric acid particles. The calculated chemical loss of column ozone assuming heterogeneous reactions on background particles is presented in Table 6 and for volcanic particles in Table 7 for March, June, September and December.

At middle latitudes, the model calculates a net ozone production, or slight reduction, in March, June and September when background particles are considered. In December, a net loss of ~15 DU is predicted. At higher latitudes, there is a net reduction in column ozone, increasing with latitude except for December.

34

Table 6:   *Monthly mean change in column ozone (DU) between 350 and 675 K including gas phase chemistry and heterogeneous reactions (R 1-R 4 and R 6-R 8) on background particles.*

Latitude	40°N	50°N	60°N	70°N	80°N
March	6.9	-6.3	-14.1	-18.3	-29.0
June	18.6	2.5	-6.5	-25.6	-38.8
September	3.1	-5.4	-11	-16.2	-22.6
December	-15.3	-16.9	-13.1	-1.3	-0.1

The introduction of volcanic particles results in higher column ozone loss compared to the background scenario. In December, the column ozone loss is increased by approximately 5 DU at 40-60°N by volcanically enhanced particles. At high latitudes there is no effect, due to low photochemical activity. The column ozone is reduced by 10 to 20 DU in September. In March, the increase in chemical loss of column ozone was approximately 10 to 30 DU. The largest loss was calculated at high latitudes. This loss is probably compensated by transport of ozone rich air from lower latitudes as transport processes govern the ozone concentration below ~20 km and poleward of 70° in the winter season (Perliski et al., 1989). The greatest effect of introducing volcanic particles is calculated in June. The added loss at middle latitudes is 15 to 20 DU. At high latitudes, the increase in column ozone loss is 30 to 50 DU. The transport into the polar region from lower latitudes is slow during the summer, and chemical ozone destruction likely plays an important role in the summer-time low observed at high latitudes. According to 2-D model calculations performed by Perliski et al. (1989), chemical processes control the ozone abundance in the lower stratosphere poleward of 50° in the summer season.

Randeniya et al. (1997) estimated a column ozone loss between 12 and 20 km at high latitudes of ~7% in June, due to chemical processes, assuming volcanically enhanced particles. They attributed half of this loss to the hydrolysis of $BrONO_2$ (R 7). The column loss calculated in this study (~70 DU) corresponds to ~20%, of which ~40% is a result of heterogeneous bromine reactions. However, the dominant reaction was the one between $BrONO_2$ and HCl, which was not included in the calculations performed by Randeniya and co-workers.

Table 7:   *Monthly mean change in column ozone (DU) between 350 and 675 K including gas phase chemistry and heterogeneous reactions (R 1-R 4 and R 6-R 8) assuming volcanically enhanced particles.*

| Latitude	40°N	50°N	60°N	70°N	80°N
March	-4.7	-22.1	-38.5	-46.6	-45.3
June	4.2	-19.1	-42.9	-76.7	-67.2
September	-6.8	-17.4	-26.7	-35.9	-39.7
December	-20.2	-21.2	-17.6	-1.6	-0.1

3.3 Proposed heterogeneous reactions

In the first section, a reaction scheme for self-activation of chlorine is presented. The results are compared to the scenario with the full heterogeneous chlorine, nitrogen and bromine reaction scheme, and to the gas phase only reaction scheme. The calculations are made for the months January through April, using two different sets of volcanically enhanced aerosol surface area densities.

The second section describes the results from implementing a reaction scheme involving nitrate radicals, which initiate a reaction sequence leading to the formation of hydrogen peroxide (H_2O_2). The results are compared to the reaction scheme with gas phase and heterogeneous chlorine, nitrogen and bromine on background and volcanic aerosols. Calculations have been made for the months of March, June, September and December.

3.3.1 Self activation of chlorine

The idea of a heterogeneous reaction between active and inactive chlorine species of the form

$R\ 9$ $ClOOCl + HCl \rightarrow Cl_2 + HOOCl$
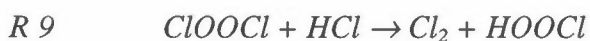
was suggested by Wofsy et al. (1988) as an acid catalysed ice surface reaction. De Haan and Birks (1997) studied the heterogeneous reactivity of ClOOCl on ice surfaces with HCl present. Cl_2 was the only gas phase product detected, whereas HOOCl has not yet been observed. Thus the existence of this reaction pathway remains uncertain. Ab initio calculations suggest that HOOCl is a stable gas phase compound (De Haan and Birks, 1997), and several pathways for further reaction such as photolysis and decomposition may exist. The impact of reaction R 9 is dependent on the fate of HOOCl and De Haan et al. (1997) suggested that the species would either decompose to HCl, or photolyse.

Reaction pathway A

R 10 $HOOCl \rightarrow HCl + O_2$

net: $ClOOCl \rightarrow Cl_2 + O_2$

Reaction pathway B

R 11 $HOOCl + h\nu \rightarrow Cl + HO_2$

net: $ClOOCl + HCl \rightarrow Cl_2 + Cl + HO_2$
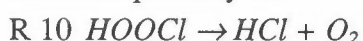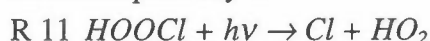
Reaction pathway B is analogous to that of either HOOH or ClOOCl (Lee and Rendell, 1993). ClOOCl undergoes thermal decomposition and is most abundant at low temperatures. It is, therefore, only present in significant amounts at high latitudes during winter. The addition of reaction R 9 represented a significant loss for ClOOCl. The absorption cross sections for ClOOCl and Cl_2 are quite similar, and when there is sufficient sunlight, both molecules will dissociate, yielding two chlorine atoms that can react with ozone. The effect of the conversion of ClOOCl to Cl_2 on the ozone concentrations is therefore minimal. Depending on the fate of HOOCl there might be an additional activation of chlorine. If HOOCl decomposes to HCl and O_2 there is no additional chlorine activation (pathway A). Alternatively, if HOOCl photolyses to Cl and HO_2 (pathway B), this will lead to added activation of chlorine.

De Haan et al. (1997) found that reaction pathway A had a negligible effect on stratospheric chlorine activation and subsequently the ozone loss rates, assuming reaction on solid PSC surfaces. Reaction pathway B was found to affect the

36

chlorine activation and ozone loss rates on realistic 10-day trajectories for the winter of 1994. Calculations over a time period of one month at fixed latitudes between 30 and 80°N on the 550 K surface were performed, assuming heterogeneous reaction on liquid sulphate particles only. The sulphate aerosol surface area densities at 550 K in 1994 were on the order of ~2 $\mu m^2 \cdot cm^{-3}$. The available reaction surfaces therefore resulted in reaction rates that were too low to significantly perturb the chlorine chemistry and enhance the amount of active chlorine.

In the present study, the effect of the heterogeneous reaction between ClOOCl and HCl on liquid sulphuric acid aerosols is investigated further, assuming that HOOCl undergoes photolysis (pathway B). The photolysis rate was set equal to that of HOCl. Calculations have been made over one month at 60, 70 and 80°N at seven isentropic surfaces for January through April. Based on the similarity between reaction R 9 and that of $ClONO_2$ with HCl (R 2), the reactive uptake coefficient was set equal to that of R 2 (De Haan et al., 1997). Reaction R 9 was added to the reaction scheme with gas phase reactions and heterogeneous chlorine, nitrogen and bromine reactions (R 1-R 4 and R 6-R 8) on volcanically enhanced liquid sulphuric acid particles. Two different sets of aerosol area densities have been used. The first set of calculations were made with particle areas observed in 1992 for the appropriate latitude, while the second set of calculations were made with an aerosol area density set equal to that at 60°N, 1992 for all latitudes. This was to ensure a maximum effect, because the sulphuric acid particles introduced into the stratosphere by the Mt. Pinatubo eruption were only present below ~450 K at high latitudes before the break-up of the polar vortex at the end of March (Neuber et al., 1994a; 1994b) (see Figure 1).

Reaction R 9 activates chlorine, resulting in a decrease in HCl concentration and an increase in ClO and subsequently also in ClOOCl. The stability of ClOOCl increases with decreasing temperature because ClOOCl undergoes thermal decomposition. ClOOCl therefore becomes more abundant with decreasing temperature and increasing latitude. There is a slight increase in the HO_X concentration through reaction R 9, but the overall concentration is not enhanced due to the reaction with ClO to form HOCl. It is therefore only the added chlorine activation that affects the net ozone loss to any significant degree.

Figure 15 (left panel) shows the difference in net ozone loss at 80°N in winter by adding reaction R 9 to the heterogeneous chlorine, bromine and nitrogen reactions, using observed particle surface area densities for the appropriate latitude. The effect of adding R 9 is negligible at 60°N, and at 70°N the additional net ozone loss amounts to 1 ppb·day⁻¹ or less (not shown). At 80°N, the added reaction has an effect only in the height region where the aerosol layer is enhanced. The aerosol layer has limited altitudinal coverage at this latitude with the maximum around 400 K (see Figure 1) where the addition of reaction R 9 has the greatest effect on net ozone loss. There is no effect above 475 K. The added ozone loss is highest in March when the combined effect of low temperatures and sunlight is most favourable to drive the photodissociation. In March, the net ozone loss at 400 K is increased by ~58%, or 15 ppb·day⁻¹ to a total of 41 ppb·day⁻¹.

The most important loss mechanism at 400 K, is the ClO-dimer cycle (L 7), which is enhanced by ~80% when reaction R 9 is added. This mechanism accounts for
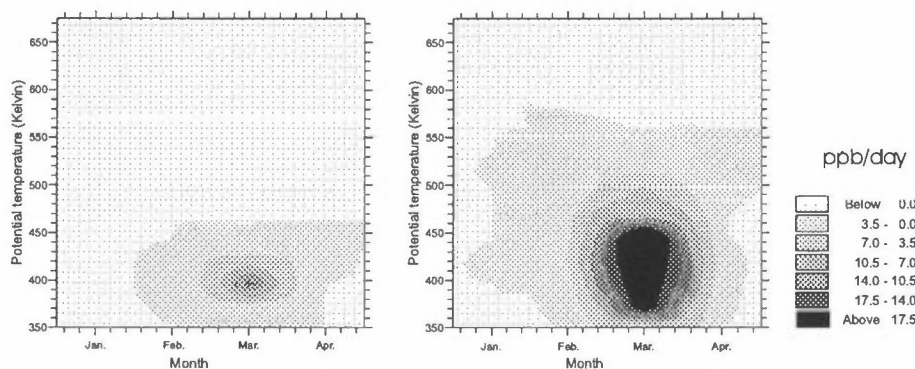
Figure 15: *The difference in net ozone loss at 80°N by adding reaction R 9 to the heterogeneous reactions R 1-R 4 and R 6-R 8. The results shown in the left panel are based on observed sulphate aerosol areas for 1992. The results shown in the right panel are based on observed particles at 60°N.*

almost twice as much of the ozone destruction as the bromine and chlorine cycle (L 6), which is the second most important loss mechanism. This mechanism is enhanced by ~30%. The only other cycle of any importance is the catalytic ClO_x cycle (L 5), which is enhanced by ~30%.

The monthly mean difference in ozone column depletion rates and reduction in column concentration by adding reaction R 9 to the heterogeneous reaction scheme is listed in Table 8. The results are given for 70 and 80°N for the months of January to April.

The fractional increase in column ozone loss is very small at 70°N, resulting in less than 2 DU loss for all months. At 80°N, the added reaction led to a 23% increase in ozone loss in March, corresponding to ~10 DU. The increased ozone depletion is a result of the added activation of chlorine and subsequent depletion of ozone.

Table 8: *Change in ozone column from 350 to 675 K by adding reaction R 9 to the scenario with heterogeneous chlorine, bromine and nitrogen reaction (R 1-R 4 and R 6-R 8) on volcanic particles, using observed particle levels for the appropriate latitude.*

Latitude	70°N		80°N	
Month	fractional increase in O_3 loss/month	diff. in O_3 column (DU/month)	fractional increase in O_3 loss/month	diff. in O_3 column (DU/month)
January	1.01	-0.1	1.00	0.0
February	1.04	-0.9	1.08	-0.6
March	1.03	-1.5	1.23	-10.5
April	1.00	-0.1	1.00	0.0

38

Figure 15 (right panel) shows the effect on net ozone loss at 80°N by adding reaction R 9, using surface area densities observed at 60°N. The effect of adding the reaction is most pronounced in March. The altitudinal extent in aerosol area density at 60°N (see Figure 1) is reflected in the net ozone loss. In the high aerosol case, the reaction rate coefficient for reaction R 9 is higher, enhancing the chlorine activation. The largest enhancement in net ozone loss is calculated at 435 K (29 ppb·day^{-1}), but the highest fractional increase is at 380 K where the additional net ozone loss is 22 ppb day^{-1}.

The difference in fractional increase in column ozone loss and the difference in the partial ozone column with and without reaction R 9 for the high aerosol scenario are given in Table 9. The difference in ozone concentration in the described height interval at 70°N is less than 3 DU for all four months. At 80°N in March the calculated ozone loss is ~50 DU over one month. This is assuming a maximum available aerosol surface.

Table 9:   As Table 8, using observed aerosol area densities at 60°N.

Latitude	70°N		80°N	
Month	fractional increase in O_3 loss/month	diff. in O_3 column (DU/month)	fractional increase in O_3 loss/month	diff. in O_3 column (DU/month)
January	1.04	-0.4	1.00	0.0
February	1.05	-1.4	1.43	-31.7
March	1.04	-2.4	1.57	-52.2
April	1.00	-0.2	1.01	-1.3

3.3.2 Liquid particle uptake of nitrate

In the night-time stratosphere, NO_X is converted to N_2O_5 which reacts on the surface of, for example, liquid sulphuric acid particles to form HNO_3 (R 4). A reaction scheme involving nitrate (NO_3) and sulphate radicals was proposed by Pedersen (1995). It has been shown that NO_3 reacts with hydrogen sulphate ions (HSO_4^-) to produce hydrogen sulphate radicals (HSO_4) (Løager et al., 1994).

R 12 $NO_3 + HSO_4^- \rightleftharpoons NO_3^- + HSO_4$

This equilibrium reaction is in competition with the formation of N_2O_5. The following fate of HSO_4 was suggested:

R 13 $2\,HSO_4 \rightleftharpoons H_2S_2O_8$

R 14 $H_2S_2O_8 + H_2O \rightleftharpoons H_2SO_5 + H_2SO_4$

R 15 $H_2SO_5 + H_2O \rightleftharpoons H_2SO_4 + H_2O_2$
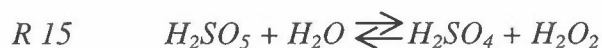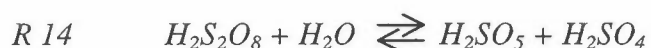
Simplified model calculations performed by Pedersen (1995) suggested that this reaction sequence could lead to a doubling of the background H_2O_2 level during

one night. It was further suggested that this increase could be accumulated, in turn leading to an increased ozone reduction in the lower stratosphere.

As a simplified approach, a net reaction, was implemented in the model.

R 16 $2\,NO_3 \rightarrow H_2O_2$
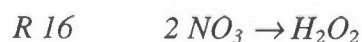
The assumption was made that the reactions R 12 through R 15 would all be shifted to the right, with no back reaction taking place. The solubility of the reaction product H_2O_2 in liquid sulphuric acid is low (Myhre and Nielsen, 1998) and H_2O_2 is, therefore, probably released to the gas phase. The reactive uptake coefficient of NO_3 onto pure water and dilute salt solutions was measured by Rudich et al. (1996). The measured uptake coefficient at 273 K was on the order of 10^{-3}. In this study, the reaction was assumed to be a temperature independent surface reaction. A reactive uptake coefficient of 0.5 was chosen in order to ensure a high effect. The reaction rate was calculated according to R 16. The reaction rate coefficient varies between $1.25 \cdot 10^{-5}$ and $2.5 \cdot 10^{-4}$ for background ($\sim 10^{-8}$ $cm^2 \cdot cm^{-3}$) and volcanic ($\sim 2 \cdot 10^{-7}$ $cm^2 \cdot cm^{-3}$) particle levels, respectively. Calculations including reaction R 16 have been made for the months of March, June September and December. Model calculations including reaction R 16 on background and volcanic aerosols were added to the simulations with heterogeneous reactions involving chlorine, bromine and nitrogen (R 1-R 4, R 6-R 8), presented in Ch. 3.2.2.

Reaction R 16 leads to an enhancement of the HO_X concentration and a reduction of NO_Y. Subsequently, the ozone loss through the catalytic HO_X cycles (L 2) is increased while the importance of the catalytic NO_X cycle (L 3) is reduced in the height region with high aerosol surface area density. The consumption of NO_3 generally leads to reduced concentrations of N_2O_5. The thermal decomposition of N_2O_5 is dependent on the concentration of N_2O_5 and the formation is governed by the concentration of NO_2 and NO_3. When an additional loss process for NO_3 is introduced, the NO_2 concentration increases. This leads to enhanced formation of $ClONO_2$ and $BrONO_2$ and subsequent decrease in ClO and BrO.

Figure 16 shows the quantitative differences in ozone loss mechanisms by adding R 16 to the heterogeneous chlorine, nitrogen and bromine reactions on background particles at 70°N in March. The heterogeneous activation is low in the case with background particles and the reaction rate coefficient for N_2O_5 hydrolysis is small. The additional HO_X produced through reaction R 16 leads to a slight enhancement of the catalytic HO_X loss cycle (L 2). At 70°N in March, the enhanced levels of NO_2 lead to an increase in $ClONO_2$ and $BrONO_2$ in the low altitude region. These two compounds react heterogeneously with HCl, leading to additional chlorine activation. Because of the low halogen activation on background particles, the additional activation leads to a small additional net ozone loss of 1-2 $ppb \cdot day^{-1}$ through the chlorine induced loss cycles (see Figure 16) at high latitudes. In all other areas and seasons the effect of the added reaction is either slightly positive or negative, but less than 0.05 $ppb \cdot day^{-1}$ and therefore negligible.
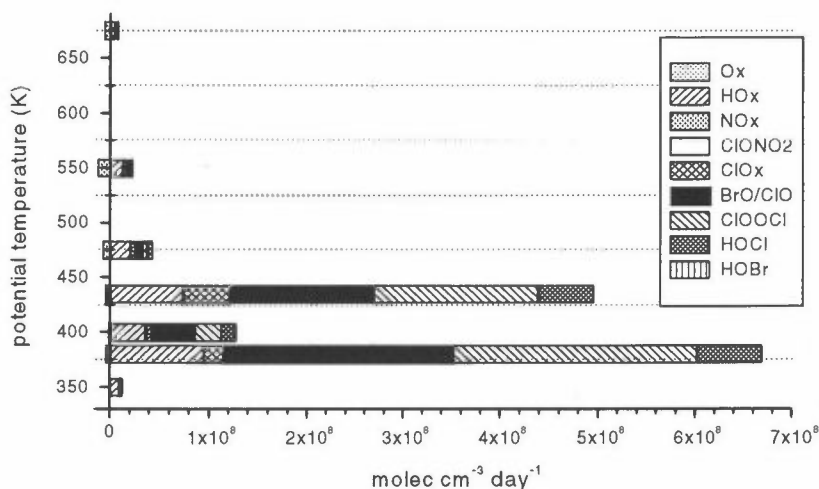
40

Figure 16: The difference in ozone loss rates (molec·cm⁻³·day⁻¹) for the different loss mechanisms at 70°N by adding R 16 to the heterogeneous chlorine, nitrogen and bromine reactions (R 1-R 4, R 6-R 8) on background particles in March.

Figure 17 shows the quantitative difference in loss cycles for ozone caused by adding reaction R 16 to the heterogeneous chlorine, nitrogen and bromine reactions on volcanic particles at 60°N in March. In this case, the heterogeneous processing of chlorine, bromine and nitrogen (R 1-R 4 and R 6-R 8) is high due to elevated particle areas. The introduction of reaction R 16 represents an additional loss process for NO_3 and subsequently reduces the N_2O_5 concentration and thereby the HNO_3 concentrations. The reaction is in competition with the N_2O_5 hydrolysis reaction (R 4) and counteracts the ozone destruction initiated by this reaction, described in Ch. 3.2.1. The loss of NO_3 and N_2O_5 leads to higher concentrations of NO_2, which reacts with ClO and BrO to form $ClONO_2$ and $BrONO_2$. The loss of HCl is generally enhanced through the reaction with $BrONO_2$ and OH, but the formation of $ClONO_2$ leads to a net deactivation of chlorine. The concentration of HOCl is reduced despite the elevated concentration of HO_X due to the reduction in active chlorine. This results in a decrease in ozone loss through the chlorine and bromine loss mechanism (L 6) and the ClO-dimer loss mechanism (L 7), and to a lesser degree, the catalytic ClO_X cycle (L 5), the HOCl photolysis mechanism (L 8) (see Figure 17). The level of H_2O_2 is enhanced, but the contribution to the production of OH and thereby HO_X is very small and the added ozone destruction through the catalytic HO_X cycle (L 2) is positive but negligible. The net ozone loss is therefore generally decreased through the addition of reaction R 16 in the volcanic case. The decrease is most pronounced in the region with the highest aerosol surface area densities.
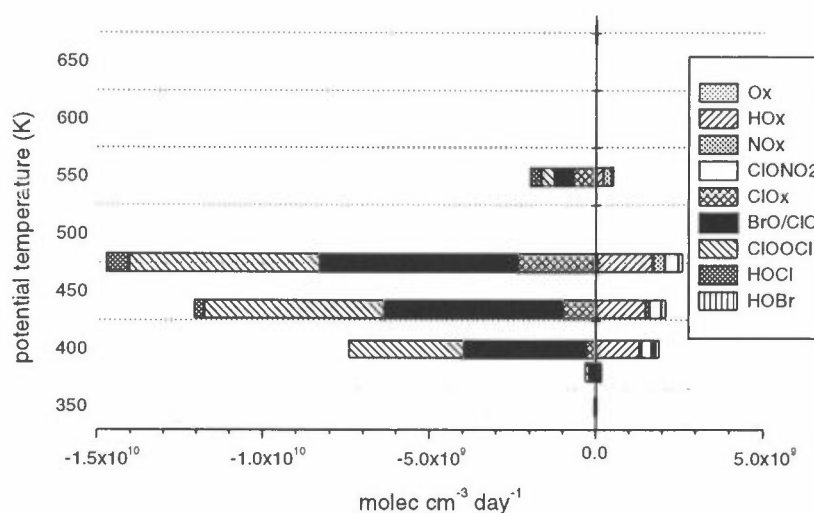
Figure 17: *The difference in ozone loss rates (molec·cm⁻³·day⁻¹) for the different loss mechanisms at 60°N by adding R 16 to the heterogeneous chlorine, nitrogen and bromine reactions (R 1-R 4, R 6-R 8) on volcanic aerosols in March.*

In March, the decrease in net ozone loss by adding reaction R 16 is most pronounced in the region with the highest aerosol surface area densities. The decrease is highest at 60°N, 475 K and amounts to ~5 ppb·day⁻¹, reducing the total net loss to 14 ppb·day⁻¹. In June, September and December, the reduction in net ozone loss is most pronounced in the area where the N_2O_5 hydrolysis is most efficient. For the latter three periods the reduction in net ozone loss amounts to ~1 ppb·day⁻¹.

4. Summary and conclusions

Heterogeneous reactions in connection with liquid sulphuric acid particles play an important role in chemical ozone depletion at middle and high latitudes in the lower stratosphere. The aim of this study was to investigate the impact of heterogeneous reaction on the partitioning of species, the ozone loss mechanisms and quantify the ozone depletion rates and the in-situ reduction of column ozone. A photochemical trajectory model has been used to study the impact of several well known and some proposed heterogeneous reactions, assuming both background and volcanically enhanced particle abundances.

The photochemical trajectory model consists of four modules which describe photodissociation, gas phase chemistry, microphysical processes leading to liquid and solid particle formation, and heterogeneous chemical reactions facilitated by particles. The modules are coupled so that the processes are subject to mutual interactions in an air parcel following the isentropic trajectories during 10-day periods. In this study, only liquid sulphuric acid particle formation was included and the model was employed as a box model.

The chemical lifetime of ozone generally decreases with the intensity of solar radiation, which increases with altitude. In the gas phase scenario, the HO_X ozone

loss cycles dominate in the lower part of the altitude range, while the catalytic NO_X becomes increasingly important with increasing altitude.

The N_2O_5 hydrolysis reaction results in a re-partitioning of the NO_Y and HO_X species. This in turn alters the relative and quantitative contribution of the catalytic NO_X and HO_X ozone loss cycles. The increase of HO_X also leads to indirect chlorine activation and subsequent enhancement of the catalytic chlorine cycle. At middle latitudes, the inclusion of the N_2O_5 hydrolysis reaction on volcanically enhanced particles led to an additional ozone loss of ~6 ppb·day^{-1} at 550 K. The resulting additional column ozone loss is 2-8 DU per month.

The heterogeneous chlorine reactions are temperature dependent, and only have an effect at high latitudes in winter. The reactions lead to direct activation of chlorine reservoir species and subsequent enhancement of the ClO-dimer ozone loss cycle, the synergetic chlorine and bromine cycle and the catalytic chlorine cycle. In March, the net ozone loss was increased by more than 10 ppb·day^{-1} at high latitudes below 435 K when volcanic particles were taken into account. This resulted in an additional in-situ column ozone loss of ~20 DU in March.

The heterogeneous bromine reactions have the greatest impact when coupled with high activation rates of chlorine. This is because ozone loss by bromine is strongly coupled to active chlorine through the chlorine and bromine loss cycle. The effect of adding heterogeneous bromine reactions was highest in June. The added column loss at middle latitudes was 4 to 16 DU per month. At high latitudes in June, the column ozone loss was increased by 30 to 50 DU.

The reaction between ClOOCl and HCl represents a pathway for self-activation of chlorine, assuming that the reaction product HOOCl undergoes photolysis. At high latitudes in winter, the reaction leads to added activation of chlorine and enhancement of the chlorine and bromine ozone loss mechanisms, particularly the ClO-dimer cycle. The effect was most pronounced in March at 80°N when there was a combination of low temperature and sufficient sunlight to drive the photo-chemistry. The model calculated an added column ozone loss of 10 DU, assuming a liquid particle loading observed at high latitudes in March 1992. Based on a particle loading observed at 60°N, the added column ozone loss was 52 DU.

The nitrate radical may be absorbed in liquid sulphuric acid particles and react through several steps, ultimately leading to the formation of H_2O_2. In this study, a simplified reaction mechanism was adopted together with a high reactive uptake coefficient. The results show that the reaction would lead to an additional ozone loss under background particle conditions, and a reduction of ozone depletion assuming volcanically enhanced particles. However, the reactive uptake coefficient assumed in this study is very high and was chosen in order to provoke a measurable effect. A more realistic consideration of solubility and temperature dependence would suggest a reactive uptake coefficient of 10^{-3}, in which case reaction R 16 would have a negligible effect on the partitioning of species and the ozone loss rate.

5. References

Bekki, S., Pyle, J.A. (1994) A 2-dimensional modeling study of the volcanic-eruption of Mount Pinatubo. *J. Geophys. Res., 99,* 18861-18869.

Bojkov, R.D., Hudson, R.D., Bishop, L., Fioletov, V. Russel III, J.M., Stolarski, R.S., Uchino, O., Zerefos, C.S. (1999) Ozone variability and trends. In: *Scientific assessment of ozone depletion: 1998.* Ed. by C.A. Ennis. Geneva (WMO, Global ozone research and monitoring project, Report no. 44), pp. 4.1-4.55.

Brühl, C., Crutzen, P.J., Grooss, J.U. (1998) High-latitude, summertime NO_x activation and seasonal ozone decline in the lower stratosphere: Model calculations based on observations by HALOE on UARS. *J. Geophys. Res., 103,* 3587-3597.

Danilin, M.Y., McConell, J.C. (1995) Stratospheric effects of bromine activation on/in sulfate aerosols. *J. Geophys. Res., 100,* 11237-11243.

De Haan, D.O. and Birks, J.W. (1997) Heterogeneous reactions of chlorine peroxide and halide ions. *J. Phys. Chem. A, 101, 43,* 8026-8034.

De Haan, D.O., Fløisand, I. and Stordal, F. (1997) Modeling studies of the effects of the heterogeneous reaction $ClOOCl + HCl \rightarrow Cl_2 + HOOCl$ on stratospheric chlorine activation and ozone depletion. *J. Geophys. Res., 102,* 1251-1258.

DeMore, W.B., Sander, S.P., Golden, D.M., Hampson, R.F., Kurylo, M.J., Howard, C.J., Ravishankara, A.R., Kolb, C.E., Molina, M.J. (1997) Chemical kinetics and photochemical data for use in stratospheric modeling. Pasadena (JPL publication 97-4).

European Commission (1997) European research in the stratosphere. The contribution of EASOE and SESAME to our current understanding of the ozone layer. Luxembourg, Office for Official Publications of the European Communities (EUR 16986).

Fløisand, I, Stordal, F., Rognerud, B., Isaksen, I.S.A., Larsen, N. and Knudsen, B. (1998) Modelled chemical ozone change over Europe during the winters 1992 to 1995. In: *Proceedings of the XVIII Quadrennial Ozone Symposium, L'Aquila, Italy, 12-21 September 1996, Vol. 2.* R.D. Bojkov and G. Visconti (ed.). L'Aquila, Parco Scientifico etecnologico d'Abruzzo. pp. 711-714.

Galle, B., Mellqvist, J., Arlander, D.W., Fløisand, I., Chipperfield, M.P., Lee, A.M. (1999) Ground based FTIR measurements of stratospheric species from Harestua, Norway during SESAME and comparison with models. *J. Atmos. Chem., 32,* 147-164.

Gleason, J.F., Bhartia, P.K., Herman, J.R., McPeters, R., Newman, P., Stolarski, R.S., Flynn, L., Labow, G., Larko, D., Seftor, C., Wellemeyer, C., Komhyr, W.D., Miller, A.J., Planet, W. (1993) Record low global ozone in 1992. *Science, 260,* 523-526.

Hanson D. R., Ravishankara A.R., Solomon S. (1994) Heterogeneous reactions in sulfuric acid aerosols: A framework for model calculations. *J. Geophys. Res., 99*, 3615-3629.

Hanson, D.R., Mauersberger, K. (1988) Laboratory studies of nitric acid trihydrate: Implications for the south polar stratosphere. *Geophys. Res. Lett., 15*, 855-858.

Harris, N.R.P., Ancellet, G., Bishop, L., Hofmann, D.J., Kerr, J.B., McPeters, R.D., Préndez, M., Randel, W., Staehelin, J., Subbaraya, B.H., Volz-Thomas, A., Zawodny, J.M., Zerefos, C.S. (1995) Ozone Measurements. In: *Scientific assessment of ozone depletion: 1994*. Ed. by C.A. Ennis. Geneva (WMO, Global ozone research and monitoring project, Report no. 37), pp. 1.1-1.54.

Hesstvedt, E., Hov, Ø., Isaksen, I.S.A. (1978) Quasi-steady-state approximations in air pollution modelling. Comparison of two numerical schemes for oxidant prediction. *Int. J. Chem. Kinet., 10*, 971-994.

Hitchman, M.H., Mckay, M., Trepte, C.R. (1994) A climatology of stratospheric aerosol. *J. Geophys. Res., 99*, 20689-20700.

Hofmann, D.J., Solomon, S. (1989) Ozone destruction through heterogeneous chemistry following the eruption of El Chichon. *J. Geophys. Res., 94*, 5029-5041.

Hofmann, D.J. (1990) Increase in the stratospheric background sulfuric acid aerosol mass in the past 10 Years. *Science, 248*, 996-1000.

Hofmann, D.J., Pyle, J.A., Austin, J., Butchart, N., Jackman, C.H., Kinnison, D.E., Lefèvre, F., Pitari, G., Shindell, D.T., Toumi, R., von der Gathen, P. (1999) Predicting future ozone changes and detection of recovery. In: *Scientific assessment of ozone depletion: 1998*. Ed. by C.A. Ennis. Geneva (WMO, Global ozone research and monitoring project, Report no. 44), pp. 12.1-12.57.

Isaksen, I.S.A., Midtbø, K.H., Sunde, J. and Crutzen, P.J. (1977) A simplified method to include molecular scattering and reflection in calculation of photon fluxes and photodissociation rates. *Geophysica Norvegica, 31*, 11-26.

Isaksen, I.S.A., Stordal, F. (1986) Antarctic ozone depletion: 2-D model studies. *Geophys. Res. Lett., 13*, 1327-1330.

Isaksen I.S.A., Rognerud, B., Stordal, F., Coffey, M.T. and Mankin, W.G. (1990) Studies of artic stratospheric ozone in a 2-D model including some effects of zonal asymmetries. *Geophys. Res. Lett., 17*, 557-560

Jackman, C.H., Fleming, E.L., Chandra, S., Considine, D.B. and Rosenfield, J.E. (1996) Past, present, and future modeled ozone trends with comparisons to observed trends. *J. Geophys. Res., 101*, 28,753-28,767.

Jones, R.L., Avallone, L., Froidevaux, L., Godin, S., Gray, L., Kinne, S., McIntyre, M.E., Newman, P.A., Plumb, R.A., Pyle, J.A., Russel III, J.M., Tolbert, M., Toumi, R., Tuck, A.F., Wennberg, P. (1995) Tropical and midlatitude ozone. In: *Scientific assessment of ozone depletion: 1994.* Ed. by C.A. Ennis. Geneva (WMO, Global ozone research and monitoring project, Report no. 37), pp. 4.1-4.38.

Johnston, P.V., McKenzie, R.L., Keys, J.G., Matthews, W.A. (1992) Observations of depleted stratospheric NO_2 following the Pinatubo volcanic-eruption. *Geophys. Res. Lett. 19,* 211-213.

Knudsen, B.M, Carver, G.D. (1994) Accuracy of the isentropic trajectories calculated for the EASOE campaign. *Geophys. Res. Lett. 21,* 1199-1203.

Knudsen, B.M., Lahoz, W.A., O'Neill, A., Morcrette, J.J. (1998) Evidence for a substantial role for dilution in northern mid-latitude ozone depletion. *Geophys. Res. Lett. 25,* 4501-4504.

Ko, M.K.W., Ibrahim, A., Isaksen, I.S.A., Jackman, C., Lefèvre, F., Prather, M., Rasch, P., Toumi, R., Visconti, G. (1995) Model simulations of stratospheric ozone. In: *Scientific assessment of ozone depletion: 1994.* Ed. by C.A. Ennis. Geneva (WMO, Global ozone research and monitoring project, Report no. 37), pp. 6.1-6.41.

Koike, M., Jones, N.B., Matthews, W.A., Johnston, P.V., McKenzie, R.L., Kinnison, D., Rodriguez, J. (1994) Impact of Pinatubo aerosols on the partitioning between NO_2 and HNO_3. *Geophys. Res. Lett. 21,* 597-600.

Larsen, N. (1991) Polar stratospheric clouds. A microphysical simulation model. Copenhagen (DMI Scientific Report 91-2).

Larsen, N., Knudsen, B.M., Rosen, J.M., Kjome, N.T., Neuber, R., Kyrö, E. (1997) Temperature histories in liquid and solid polar stratospheric cloud formation. *J. Geophys. Res., 102,* 23505-23517.

Lee, T.J., Rendell, A.P. (1993) Ab-initio characterization of ClOOH – implications for atmospheric chemistry. *J. Phys. Chem., 97,* 6999-7002.

Løgager, T., Sehested, K., Holcman, J. (1993) Rate constants of the equilibrium reactions $SO_4^- + HNO_3 \rightleftharpoons HSO_4^- + NO_3$ and $SO_4^- + NO_3^- \rightleftharpoons SO_4^{2-} + NO_3$. *Radiat. Phys. Chem., 41,* 539-543.

Manney, G.L., Santee, M.L., Froidevaux, L., Waters, J.W., Zurek, R.W. (1996) Polar vortex conditions during the 1995-96 Arctic winter: Meteorology and MLS ozone. *Geophys. Res. Lett., 23,* 3203-3206.

Marti, J., Mauersberger, K. (1993) A survey and new measurements of ice vapour pressure at temperatures between 170 and 250 K. *Geophys. Res. Lett., 20,* 363-366.

McCormick, M.P., Trepte, C.R., Pitts, M.C. (1989) Persistence of polar stratospheric clouds in the southern polar-region. *J. Geophys. Res., 94,* 11241-11251.

Myhre, C.E.L., Nielsen, C.J. (1998) Interaction between H_2O_2 and cold sulfuric acid: Uptake measurements and Henry's law constant. In: *Polar stratospheric ozone 1997. Proceedings of the fourth European symposium, 22 to 26 Sept. 1997, Schliersee, Bavaria, Germany.* Brussels, European Commission (Air pollution research report 66). pp.589-592.

Neuber, R., Beyerle, G., Fiocco, G., Disarra, A., Fricke, K.H., David, C., Godin, S., Knudsen, B.M., Stefanutti, L., Vaughan, G., Wolf, J.P. (1994a) Latitudinal distribution of stratospheric aerosols during the EASOE winter 1991/92. *Geophys. Res. Lett. 21*, 1283-1286.

Neuber, R., Beyerle, G., Schrems, O., Fabian, R., von der Gathen, P., Krüger, B.C. (1994b) Measurements of stratospheric ozone and aerosols above Spitsbergen. In: *Proceedings of the XVII Quadrennial ozone symposium, Charlottesville, Virginia, 4-13 June 1992, Vol. 2.* R.D. Hudson (ed.). (NASA Conference Publication 3266).

Park J.H., Russell III, J.M. (1994) Summer polar chemistry observations in the stratosphere made by HALOE. *J. Atmos. Sci., 51*, 677-693.

Pedersen, T. (1995) Nighttime hydrogen-peroxide production on sulfuric-acid-aerosols involving nitrate and sulfate radicals. *Geophys. Res. Lett. 22*, 1497-1499.

Perliski, L.M., Solomon, S., London, J. (1989) On the interpretation of seasonal-variations of stratospheric ozone. *Planet. Space. Sci., 37*, 1527-1538.

Pitari, G., Rizi, V. (1993) An estimate of the chemical and radiative perturbation of stratospheric ozone following the eruption of Mt. Pinatubo. *J. Atmos. Sci., 50*, 3260-3276.

Randeniya, L.K., Vohralik, P.F., Plumb, I.C., Ryan, K.R. (1997) Heterogenous $BrONO_2$ hydrolysis: Effect on NO_2 columns and ozone at high latitudes in summer. *J. Geophys. Res., 102*, 23543-23557.

Ravishankara, A.R., Shepherd, T.G., Chipperfield, M.P., Haynes, P.H., Kawa, S.R., Peter, T., Plumb, R.A., Portmann, R.W., Randel, W.J., Waugh, D.W., Worsnop, D.R. (1999) Lower stratospheric processes. In: *Scientific assessment of ozone depletion: 1998.* Ed. by C.A. Ennis. Geneva (WMO, Global ozone research and monitoring project, Report no. 44), pp. 7.1-7.76.

Reid, S.J., Rex, M., Gathen, P. von der, Fløisand, I., Stordal, F., Carver, G.D., Beck, A., Reimer, E., Krüger-Carstensen, R., de Haan, L.L., Braathen, G., Dorokhov, V., Fast, H., Kyrö, E., Gil, M., Lityñska, Z., Molyneux, M., Murphy, G., O'Connor, F., Ravegnani, F., Varotsos, C., Wenger, J. and Zerefos, C. (1998) A study of ozone laminae using diabatic trajectories, contour advection and photochemical trajectory model simulations. *J. Atmos. Chem., 30*, 187-207.

Rex, M., Harris, NR.P., von der Gathen, P., Lehmann, R., Braathen, G.O., Reimer, E., Beck, A., Chipperfield, M.P., Alfier, R., Allaart, M., O'Connor, F., Dier, H., Dorokhov, V., Fast, H., Gil, M., Kyrö, E., Litynska, Z., Mikkelsen,

I.S., Molyneux, M.G., Nakane, H., Notholt, J., Rummukainen, M., Viatte, P., Wenger, J. (1997) Prolonged stratospheric ozone loss in the 1995-96 Arctic winter. *Nature, 389*, 835-838.

Rinsland, C.P., Gunson, M.R., Abrams, M.C., Lowes, L.L., Zander, R., Mahieu, E., Goldman, A., Ko, M.K.W., Rodriguez, J.M., Sze, N.D. (1994) Heterogeneous conversion of N_2O_5 to HNO_3 in the post-Mt. Pinatubo eruption stratosphere. *J. Geophys. Res., 99*, 8213-8219.

Rosenfield, J.E., Considine, D.B., Meade, P.E., Bacmeister, J.T., Jackman, C.H. and Schoeberl, M.R. (1997) Stratospheric effects of Mount Pinatubo aerosol studied with a coupled two-dimensional model. *J. Geophys. Res., 102*, 3649-3670.

Rudich, Y., Talukdar, R.K., Ravishankara, A.R. (1996) Reactive uptake of NO_3 on pure water and ionic solutions. *J. Geophys. Res., 101*, 21023-321031.

Solomon, S., Portmann, R.W., Garcia, R.R., Thomason, L.W., Poole, L.R., McCormick, M.P. (1996) The role of aerosol variations in anthropogenic ozone depletion at northern midlatitudes. *J. Geophys. Res., 101,* 6713-6727.

Solomon, S., Portmann, R.W., Garcia, R.R., Randel, W., Wu, F., Nagatani, R., Gleason, J., Thomason, L., Poole, L.R., McCormick, M.P. (1998) Ozone depletion at mid-latitudes: Coupling of volcanic aerosols and temperature variability to anthropogenic chlorine. *Geophys. Res. Lett, 25*, 1871-1874.

Stordal, F., Isaksen, I.S.A. and Horntvedt, K. (1985) A diabatic circulation two-dimensional model with photochemistry: simulations of ozone and long-lived tracers with surface sources. *J. Geophys. Res., 90*, 5757-5776.

Stordal, F., Isaksen, I.S.A. (1987) Ozone perturbation due to increases in N_2O, CH_4 and chlorocarbons: two-dimensional time-dependent calculations. *Tellus, 39B*, 333-353.

Tie, X.-X., Brasseur, G.P., Briegleb, B., Granier, C. (1994) 2-dimensional simulation of Pinatubo aerosol and its effect on stratospheric ozone. *J. Geophys. Res., 99*, 20545-20562.

Thomason, L.W., Poole, L.R., Deshler, T. (1997a) A global climatology of stratospheric aerosol surface area density deduced from stratospheric aerosol and gas experiment II measurements: 1984-1994. *J. Geophys. Res., 102*, 8967-8976.

Thomason, L.W., Kent, G.S., Trepte, C.R., Poole, L.R. (1997b) A comparison of the stratospheric aerosol background periods of 1979 and 1989-1991. *J. Geophys. Res., 102*, 3611-3616.

Turco R. P., Toon O. B., Hamill P. (1989) Heterogeneous physicochemistry of the polar ozone hole. *J. Geophys. Res., 94*, 16493-16510.

Wofsy, SC., Molina, M.J., Salawitch, R.J., Fox, L.E., McElroy, M.B. (1988) Interactions between HCl, NO_x, and H_2O ice in the Antarctic stratosphere - Implications for ozone. *J. Geophys. Res., 93*, 2442-2450.

Zerefos, CS., Tourpali, K., Bojkov, B.R., Balis, D.S., Rognerud, B., Isaksen, I.S.A. (1997) Solar activity total column ozone relationships: Observations and model studies with heterogeneous chemistry. *J. Geophys. Res., 102*, 1561-1569.

Appendix A

Reaction rates

Table A.1: Photolysis reactions.

Reaction	Comments	Ref. in chem. scheme
$O_2 + h\nu \rightarrow 2\,O$		J1
$O_3 + h\nu \rightarrow O_2 + O(^1D)$	Temperature dependent	J2
$O_3 + h\nu \rightarrow O_2 + O(^3P)$	Temperature dependent	J3
$H_2O + h\nu \rightarrow OH + H$		J4
$H_2O_2 + h\nu \rightarrow 2\,OH$	Temperature dependent	J5
$HNO_3 + h\nu \rightarrow NO_2 + OH$	Temperature dependent	J6
$HNO_2 + h\nu \rightarrow NO + OH$		J7
$HO_2NO_2 + h\nu \rightarrow NO_2 + HO_2$		J8
$N_2O + h\nu \rightarrow N_2 + O$		J9
$NO_2 + h\nu \rightarrow NO + O$		J10
$NO_3 + h\nu \rightarrow NO_2 + O$		J11
$N_2O_5 + h\nu \rightarrow NO_2 + NO_3$	Temperature dependent	J12
$CH_2O + h\nu \rightarrow H + HCO$		J13
$CH_2O + h\nu \rightarrow H_2 + CO$		J14
$CF_2Cl_2 + h\nu \rightarrow Cl_X$	Temperature dependent	J15
$CFCl_3 + h\nu \rightarrow Cl_X$	Temperature dependent	J16
$CCl_4 + h\nu \rightarrow Cl_X$		J17
$CHF_2Cl + h\nu \rightarrow Cl_X$		J18
$CH_3Cl + h\nu \rightarrow Cl_X$		J19
$ClONO_2 + h\nu \rightarrow Cl + NO_3$ $ClONO_2 + h\nu \rightarrow ClO + NO_2$	Temperature dependent, ε for channel 1 is 2/9	J20
$HOCl + h\nu \rightarrow OH + Cl$		J21
$CH_3OOH + h\nu \rightarrow CH_3O + OH$		J22
$HCl + h\nu \rightarrow H + Cl$		J23
$ClO + h\nu \rightarrow Cl + O$		J24
$CH_3CCl_3 + h\nu \rightarrow Cl_X$		J25
$OClO + h\nu \rightarrow O + ClO$		J26
$Cl_2 + h\nu \rightarrow 2\,Cl$	Temperature dependent	J27
$BrO + h\nu \rightarrow Br + O$		J28
$BrONO_2 + h\nu \rightarrow Br + NO_3$		J29
$Br_2 + h\nu \rightarrow 2\,Br$		J30
$HBr + h\nu \rightarrow H + Br$		J31
$HOBr + h\nu \rightarrow OH + Br$		J32
$CH_3Br + h\nu \rightarrow Br_Y$		J33
$CF_2ClBr + h\nu \rightarrow Br_Y$		J34
$CF_3Br + h\nu \rightarrow Br_Y$		J35
$C_2Br_2F_4 + h\nu \rightarrow Br_Y$		J36
$C_2F_3Cl_3 + h\nu \rightarrow Cl_X$		J37
$C_2F_4Cl_2 + h\nu \rightarrow Cl_X$		J38

Reaction	Comments	Ref. in chem. scheme
$C_2F_5Cl + h\nu \rightarrow Cl_X$		J39
$Cl_2O_2 + h\nu \rightarrow ClOO + Cl$		J40
$BrCl + h\nu \rightarrow Br + Cl$	Temperature dependent	J41
$CHCl_2CF_3 + h\nu \rightarrow Cl_X$		J42
$CH_3CCl_2F + h\nu \rightarrow Cl_X$		J43
$CH_3CClF_2 + h\nu \rightarrow Cl_X$		J44
$NO + h\nu \rightarrow N + O$		J45
$HOOCl + h\nu \rightarrow Cl + HO_2$	Set equal to J21	J46

Table A.2: Temperature independent bimolecular gas phase reactions.

Reaction	Rate coefficient	Ref. in chem. scheme
$O(^1D) + N_2O \rightarrow N_2 + O_2$	$4.9 \cdot 10^{-11}$	C213A
$O(^1D) + N_2O \rightarrow 2\ NO$	$6.7 \cdot 10^{-11}$	C213B
$O(^1D) + H_2 \rightarrow OH + H$	$1.1 \cdot 10^{-10}$	C221
$O(^1D) + H_2O \rightarrow OH + OH$	$2.2 \cdot 10^{-10}$	C222
$O(^1D) + CH_4 \rightarrow OH + CH_3$	$1.35 \cdot 10^{-10}$	C256
$O(^1D) + CH_4 \rightarrow H_2 + CH_2O$	$1.5 \cdot 10^{-11}$	C256A
$O(^1D) + CFCl_3 \rightarrow Cl_X$	$2.3 \cdot 10^{-10}$	C261A
$O(^1D) + CF_2Cl_2 \rightarrow Cl_X$	$1.4 \cdot 10^{-10}$	C261B
$O(^1D) + HCl \rightarrow Cl + OH$	$1.5 \cdot 10^{-10}$	C239
$OH + CH_2O \rightarrow H_2O + HCO$	$1.0 \cdot 10^{-11}$	C1948
$BrO + HO_2 \rightarrow HOBr + O_2$	$5.0 \cdot 10^{-12}$	C51I
$BrO + OH \rightarrow Br + HO_2$	$7.5 \cdot 10^{-11}$	C51K
$OH + HBr \rightarrow H_2O + Br$	$1.1 \cdot 10^{-11}$	C52A
$Br_2 + OH \rightarrow HOBr + Br$	$4.2 \cdot 10^{-11}$	C53A

Table A.3: Temperature dependent bimolecular gas phase reactions.

Reaction	Reaction rate coefficient	Ref. in chem. scheme
$N + NO \rightarrow N_2 + O$	$2.1 \cdot 10^{-11} \cdot e^{100/T}$	RC1
$N + O_2 \rightarrow NO + O$	$1.5 \cdot 10^{-11} \cdot e^{-3600/T}$	RC2
$O(^3P) + O_3 \rightarrow 2\ O_2$	$8.0 \cdot 10^{-12} \cdot e^{-2060/T}$	C107
$O(^3P) + NO_2 \rightarrow NO + O_2$	$6.5 \cdot 10^{-12} \cdot e^{+120/T}$	C110
$O(^3P) + ClO \rightarrow Cl + O_2$	$3.0 \cdot 10^{-11} \cdot e^{70/T}$	C136
$O(^3P) + HCl \rightarrow OH + Cl$	$1.0 \cdot 10^{-11} \cdot e^{-3300/T}$	C139
$O(^3P) + ClONO_2 \rightarrow NO_3 + ClO$	$2.9 \cdot 10^{-12} \cdot e^{-800/T}$	C143A
$O(^3P) + OH \rightarrow O_2 + H$	$2.2 \cdot 10^{-11} \cdot e^{120/T}$	R119
$O(^3P) + HO_2 \rightarrow OH + O_2$	$3.0 \cdot 10^{-11} \cdot e^{200/T}$	R120

Reaction	Reaction rate coefficient	Ref. in chem. scheme
$O(^3P) + CH_2O \rightarrow HCO + OH$	$3.4 \cdot 10^{-11} \cdot e^{-1600/T}$	R148
$O(^1D) + N_2 \rightarrow O(^3P) + N_2$, $\mu_{N_2}=0.7809$ $O(^1D) + O_2 \rightarrow O(^3P) + O_2$, $\mu_{O_2}=0.2095$	$0.7809 * 1.8 \cdot 10^{-11} \cdot e^{+110/T} +$ $0.2095 * 3.2 \cdot 10^{-11} \cdot e^{+70/T}$	R2M
$O_3 + NO \rightarrow NO_2 + O_2$	$2.0 \cdot 10^{-12} \cdot e^{-1400/T}$	C709
$O_3 + H \rightarrow OH + O_2$	$1.4 \cdot 10^{-10} \cdot e^{-470/T}$	C718
$O_3 + NO_2 \rightarrow NO_3 + O_2$	$1.2 \cdot 10^{-13} \cdot e^{-2450/T}$	C710
$O_3 + OH \rightarrow HO_2 + O_2$	$1.6 \cdot 10^{-12} \cdot e^{-940/T}$	C719
$O_3 + HO_2 \rightarrow OH + 2 O_2$	$1.1 \cdot 10^{-14} \cdot e^{-500/T}$	C720
$O_3 + Cl \rightarrow ClO + O_2$	$2.9 \cdot 10^{-11} \cdot e^{-260/T}$	C735
$NO + NO_3 \rightarrow 2 NO_2$	$1.5 \cdot 10^{-11} \cdot e^{170/T}$	C911
$NO + HO_2 \rightarrow NO_2 + OH$	$3.5 \cdot 10^{-12} \cdot e^{250/T}$	C920
$NO + ClO \rightarrow NO_2 + Cl$	$6.4 \cdot 10^{-12} \cdot e^{290/T}$	C936
$NO + CH_3O_2 \rightarrow CH_3O + NO_2$	$3.0 \cdot 10^{-12} \cdot e^{280/T}$	R951C
$NO_2 + NO_3 \rightarrow NO + NO_2 + O_2$	$4.5 \cdot 10^{-14} \cdot e^{-1260/T}$	C1011
$OH + OH \rightarrow H_2O + O(^3P)$	$4.2 \cdot 10^{-12} \cdot e^{-240/T}$	C1919
$OH + HO_2 \rightarrow H_2O + O_2$	$4.8 \cdot 10^{-11} \cdot e^{250/T}$	R1920
$OH + H_2 \rightarrow H_2O + H$	$5.5 \cdot 10^{-12} \cdot e^{-2000/T}$	C1921
$OH + H_2O_2 \rightarrow H_2O + HO_2$	$2.9 \cdot 10^{-12} \cdot e^{-160/T}$	C1923
$OH + HNO_2 \rightarrow H_2O + NO_2$	$1.8 \cdot 10^{-11} \cdot e^{-390/T}$	C1925
$OH + HNO_3 \rightarrow H_2O + NO_3$	$C0 + C3M/(1. + C3M/C2)$ $C0 = 7.2 \cdot 10^{-15} \cdot e^{+785/T}$ $C2 = 4.1 \cdot 10^{-16} \cdot e^{+1440/T}$ $C3M = 1.9 \cdot 10^{-33} \cdot e^{+725/T}) \cdot [M]$	C1926
$OH + ClO \rightarrow HO_2 + Cl$	$1.1 \cdot 10^{-11} \cdot e^{120/T}$	C1936
$OH + CH_3OOH \rightarrow CH_3O_2 + H_2O$	$3.8 \cdot 10^{-12} \cdot e^{200/T}$	C19CX
$OH + HOCl \rightarrow H_2O + ClO$	$3.0 \cdot 10^{-12} \cdot e^{-500/T}$	C1937
$OH + HCl \rightarrow H_2O + Cl$	$2.6 \cdot 10^{-12} \cdot e^{-350/T}$	C1939
$OH + CO \rightarrow CO_2 + H$	$1.5 \cdot 10^{-13} (1. + 0.6 \cdot [M]/2.5 \cdot 10^{19})$	C1945
$OH + CH_4 \rightarrow CH_3 + H_2O$	$2.45 \cdot 10^{-12} \cdot e^{-1775/T}$	C1956
$OH + CH_3Cl \rightarrow CH_2Cl + H_2O$	$4.0 \cdot 10^{-12} \cdot e^{-1400/T}$	C1961C
$OH + CH_3CCl_3 \rightarrow CH_2CCl_3 + H_2O$	$1.8 \cdot 10^{-12} \cdot e^{-1550/T}$	C1965A
$OH + CHF_2Cl \rightarrow CF_2Cl + H_2O$	$1.0 \cdot 10^{-12} \cdot e^{-1600/T}$	C1965B
$OH + ClONO_2 \rightarrow HOCl + NO_3$	$1.2 \cdot 10^{-12} \cdot e^{-330/T}$	C1943A
$OH + HO_2NO_2 \rightarrow O_2 + H_2O + NO_2$	$1.3 \cdot 10^{-12} \cdot e^{380/T}$	R191020
$HO_2 + HO_2 \rightarrow H_2O_2 + O_2$ $HO_2 + HO_2 + M \rightarrow H_2O_2 + O_2 + M$	$2.3 \cdot 10^{-13} \cdot e^{600/T} +$ $1.7 \cdot 10^{-33} \cdot e^{1000/T} \cdot [M]$	R2020
$HO_2 + Cl \rightarrow HCl + O_2$	$1.8 \cdot 10^{-11} \cdot e^{170/T}$	R2035
$HO_2 + Cl \rightarrow OH + ClO$	$4.1 \cdot 10^{-11} \cdot e^{-450/T}$	R2035B
$HO_2 + ClO \rightarrow HOCl + O_2$	$4.8 \cdot 10^{-13} \cdot e^{700/T}$	R2036
$HO_2 + CH_3O_2 \rightarrow CH_3OOH + O_2$	$3.8 \cdot 10^{-13} \cdot e^{800/T}$	R2051
$H_2 + Cl \rightarrow HCl + H$	$3.7 \cdot 10^{-11} \cdot e^{-2300/T}$	C2135
$H_2O_2 + Cl \rightarrow HCl + HO_2$	$1.1 \cdot 10^{-11} \cdot e^{-980/T}$	C2335

Reaction	Reaction rate coefficient	Ref. in chem. scheme
$Cl + CH_4 \rightarrow HCl + CH_3$	$1.1 \cdot 10^{-11} \cdot e^{-1400/T}$	C3556
$Cl + CH_2O \rightarrow HCl + HCO$	$8.1 \cdot 10^{-11} \cdot e^{-30/T}$	C3548
$Cl + ClONO_2 \rightarrow Cl_2 + NO_3$	$6.5 \cdot 10^{-12} \cdot e^{135/T}$	C3543A
$ClO + CO \rightarrow Cl + CO_2$	$1.0 \cdot 10^{-12} \cdot e^{-3700/T}$	C3645
$Br + O_3 \rightarrow BrO + O_2$	$1.7 \cdot 10^{-11} \cdot e^{-800/T}$	C50A
$Br + H_2O_2 \rightarrow HBr + HO_2$	$1.0 \cdot 10^{-11} \cdot e^{-3000/T}$	C50B
$Br + CH_2O \rightarrow HBr + HCO$	$1.7 \cdot 10^{-11} \cdot e^{-800/T}$	C50C
$Br + HO_2 \rightarrow HBr + O_2$	$1.5 \cdot 10^{-11} \cdot e^{-600/T}$	C50D
$BrO + O(^3P) \rightarrow Br + O_2$	$1.9 \cdot 10^{-11} \cdot e^{230/T}$	C51A
$BrO + ClO \rightarrow Br + OClO$	$1.6 \cdot 10^{-12} \cdot e^{430/T}$	C51B
$BrO + ClO \rightarrow BrCl + O_2$	$5.8 \cdot 10^{-13} \cdot e^{170/T}$	C51L
$BrO + ClO \rightarrow Br + ClOO$	$2.9 \cdot 10^{-12} \cdot e^{220/T}$	C51C
$BrO + NO \rightarrow NO_2 + Br$	$8.8 \cdot 10^{-12} \cdot e^{260/T}$	C51D
$BrO + BrO \rightarrow 2\, Br + O_2$	$2.4 \cdot 10^{-12} \cdot e^{40/T}$	C51F
$BrO + BrO \rightarrow Br_2 + O_2$	$2.8 \cdot 10^{-14} \cdot e^{860/T}$	C51G
$BrO + O_3 \rightarrow Br + 2O_2$	$1.0 \cdot 10^{-12} \cdot e^{-3200/T}$	C51H
$O + HBr \rightarrow OH + Br$	$5.8 \cdot 10^{-12} \cdot e^{-1500/T}$	C52B
$OClO + NO \rightarrow NO_2 + ClO$	$2.5 \cdot 10^{-12} \cdot e^{-600/T}$	C60A
$OClO + O(^3P) \rightarrow ClO + O_2$	$2.4 \cdot 10^{-12} \cdot e^{-960/T}$	C60B
$OH + CH_3Br \rightarrow CH_2Br + H_2O$	$4.0 \cdot 10^{-12} \cdot e^{-1470/T}$	C19MBR

Table A.4: Termolecular reactions.

Reaction	k_0^{300}	n	k_∞^{300}	m	Ref. in chem. scheme
$NO_2 + OH + M \rightarrow HNO_3 + M$	$2.5 \cdot 10^{-30}$	4.4	$1.6 \cdot 10^{-11}$	1.7	C1019X
$O(^3P) + NO_2 + M \rightarrow NO_3 + M$	$9.0 \cdot 10^{-32}$	2.0	$2.2 \cdot 10^{-11}$	0.0	C110M
$OH + OH + M \rightarrow H_2O_2 + M$	$6.2 \cdot 10^{-31}$	1.0	$2.6 \cdot 10^{-11}$	0.0	C1919M
$NO + OH + M \rightarrow HONO + M$	$7.0 \cdot 10^{-31}$	2.6	$3.6 \cdot 10^{-11}$	0.1	C919M
$NO_2 + ClO + M \rightarrow ClONO_2 + M$	$1.8 \cdot 10^{-31}$	3.4	$1.5 \cdot 10^{-11}$	1.9	C1036M
$O(^3P) + O_2 + M \rightarrow O_3 + M$	$6.0 \cdot 10^{-34}$	2.3	0.0	0.0	C104M
$O_2 + H + M \rightarrow HO_2 + M$	$5.7 \cdot 10^{-32}$	1.6	$7.5 \cdot 10^{-11}$	0.0	C418M
$BrO + NO_2 + M \rightarrow BrONO_2 + M$	$5.2 \cdot 10^{-31}$	3.2	$6.9 \cdot 10^{-12}$	2.9	C51E
$ClO + ClO + M \rightarrow Cl_2O_2 + M$	$2.2 \cdot 10^{-32}$	3.1	$3.5 \cdot 10^{-12}$	1.0	C36M
$Cl + O_2 + M \rightarrow ClOO + M$	$2.7 \cdot 10^{-33}$	1.5	0.0	0.0	C3504
$NO_2 + NO_3 + M \rightarrow N_2O_5 + M$	$2.2 \cdot 10^{-30}$	3.9	$1.5 \cdot 10^{-12}$	0.7	C1011X
$NO_2 + HO_2 + M \rightarrow HO_2NO_2 + M$	$1.8 \cdot 10^{-31}$	3.2	$4.7 \cdot 10^{-12}$	1.4	C1020

Table A.5: Thermal decomposition reactions.

Reaction	Rate coefficient	Ref. in chem. scheme
$Cl_2O_2 \rightarrow ClO + ClO$	$C36M/(1.3 \cdot 10^{-27} \cdot e^{8744/T})$	C61B
$ClOO \rightarrow Cl + O_2$	$C3504/(5.7 \cdot 10^{-25} \cdot e^{2500/T})$	C61A
$N_2O_5 \rightarrow NO_2 + NO_3$	$C1011X/(2.7 \cdot 10^{-27} \cdot e^{11000/T})$	C14M
$HO_2NO_2 \rightarrow HO_2 + NO_2$	$C1020/(2.1 \cdot 10^{-27} \cdot e^{10900/T})$	CC1020

Table A.6: Reactive uptake coefficient for heterogeneous reactions on solid particles.

Reaction	SAT	NAT	ice	Ref. in chem. scheme
$ClONO_2 + H_2O \rightarrow HOCl + HNO_3$	a	10^{-3}	0.3	BDPAR
$ClONO_2 + HCl \rightarrow ClNO_2 + HNO_3$	b	0.1	0.3	BCPAR
$HOCl + HCl \rightarrow Cl_2 + H_2O$	-	0.1	0.3	ECPAR
$N_2O_5 + H_2O \rightarrow 2 HNO_3$	$6 \cdot 10^{-3}$	$3 \cdot 10^{-4}$	0.01	ADPAR
$N_2O_5 + HCl \rightarrow ClNO_2 + HNO_3$	-	$3 \cdot 10^{-3}$	0.03	ACPAR
$HOBr + HCl \rightarrow BrCl + H_2O$	-	0.1	0.3	GCPAR
$BrONO_2 + H_2O \rightarrow HOBr + HNO_3$	-	0.1	0.3	IDPAR
$BrONO_2 + HCl \rightarrow BrCl + HNO_3$	-	-	-	ICPAR

a parameterisation taken from DeMore et al., 1997, table 64, note 46
b parameterisation taken from DeMore et al., 1997, table 64, note 51

Table A.7: Reactive uptake coefficient for heterogeneous reactions in or on liquid particles.

Reaction	Reactive uptake coefficient (γ)	Ref. in chem. scheme
$ClONO_2 + H_2O \rightarrow HOCl + HNO_3$	a	BDPARBK
$ClONO_2 + HCl \rightarrow ClNO_2 + HNO_3$	a	BCPARBK
$HOCl + HCl \rightarrow Cl_2 + H_2O$	a	ECPARBK
$N_2O_5 + H_2O \rightarrow 2 HNO_3$	0.1	ADPARBK
$N_2O_5 + HCl \rightarrow ClNO_2 + HNO_3$	-	ACPARBK
$HOBr + HCl \rightarrow BrCl + H_2O$	b	GCPARBK
$BrONO_2 + H_2O \rightarrow HOBr + HNO_3$	0.8	IDPARBK
$BrONO_2 + HCl \rightarrow BrCl + HNO_3$	0.9	ICPARBK

a parameterised according to Hansen et al., 1994
b parameterised as liquid phase reaction (Danilin and McConnell, 1995)

Appendix B

Monthly mean temperatures

Mean temperature ($\overline{T}$) and standard deviation (σ) for January 1997.
Units: Kelvin (K).

λ	350 K		380 K		400 K		435 K		475 K		550 K		675 K	
	$\overline{T}$	σ	$\overline{T}$	σ	$\overline{T}$	σ	$\overline{T}$	σ	$\overline{T}$	σ	$\overline{T}$	σ	$\overline{T}$	σ
40	218.2	6.4	218.2	5.3	216.4	4.9	214.7	4.8	213.9	4.4	215.7	3.8	219.7	4.1
50	217.9	5.6	218.8	5.2	218.1	5.3	216.8	6.0	215.6	6.4	216.2	7.3	218.2	8.6
60	216.7	4.9	216.8	5.3	215.8	5.9	214.1	7.3	212.8	8.3	211.8	10.4	212.3	12.3
70	215.0	4.4	213.0	5.0	211.2	5.8	208.3	7.4	206.4	8.6	204.4	10.6	204.3	12.7
80	213.6	3.2	209.4	3.5	207.0	3.7	203.0	4.7	200.3	5.5	198.0	6.4	197.6	8.5

Mean temperature ($\overline{T}$) and standard deviation (σ) for February 1997.
Units: Kelvin (K).

λ	350 K		380 K		400 K		435 K		475 K		550 K		675 K	
	$\overline{T}$	σ	$\overline{T}$	σ	$\overline{T}$	σ	$\overline{T}$	σ	$\overline{T}$	σ	$\overline{T}$	σ	$\overline{T}$	σ
40	219.3	6.5	218.5	5.5	216.1	5.1	214.3	4.6	213.8	3.6	215.4	2.9	218.6	2.9
50	219.2	5.1	220.3	4.4	219.5	4.4	218.3	4.8	217.1	4.9	217.2	5.5	218.3	6.0
60	217.5	4.8	217.2	5.3	216.4	5.6	215.1	6.5	214.0	7.0	213.7	7.9	214.9	8.1
70	211.9	4.4	209.4	5.9	208.0	6.4	205.5	7.7	204.4	8.2	205.2	8.1	207.5	7.8
80	206.9	3.9	202.7	3.8	200.7	4.1	197.1	4.8	195.6	4.5	196.7	4.6	199.4	5.5

Mean temperature ($\overline{T}$) and standard deviation (σ) for March 1997.
Units: Kelvin (K).

λ	350 K		380 K		400 K		435 K		475 K		550 K		675 K	
	$\overline{T}$	σ	$\overline{T}$	σ	$\overline{T}$	σ	$\overline{T}$	σ	$\overline{T}$	σ	$\overline{T}$	σ	$\overline{T}$	σ
40	219.1	6.1	218.7	4.5	216.3	3.8	214.5	3.0	214.4	2.5	216.1	2.2	219.7	2.8
50	220.1	5.6	221.0	4.6	219.8	4.1	218.5	3.9	217.7	3.6	217.7	3.9	219.1	5.2
60	217.0	5.0	217.2	5.3	216.5	5.3	215.6	5.6	215.1	5.6	215.0	5.9	216.4	6.6
70	210.4	4.6	207.8	5.1	206.7	5.3	205.4	6.0	205.0	6.3	207.1	6.1	211.5	5.9
80	204.2	2.8	200.6	2.6	199.1	2.8	197.2	3.0	197.0	2.8	200.6	3.3	206.9	3.7

Mean temperature ($\overline{T}$) and standard deviation (σ) for April 1997.
Units: Kelvin (K).

λ	350 K		380 K		400 K		435 K		475 K		550 K		675 K	
	$\overline{T}$	σ	$\overline{T}$	σ	$\overline{T}$	σ	$\overline{T}$	σ	$\overline{T}$	σ	$\overline{T}$	σ	$\overline{T}$	σ
40	219.1	5.5	219.4	4.4	216.9	3.6	214.6	2.9	214.6	2.3	216.2	1.7	220.1	1.8
50	220.2	5.2	221.6	4.6	220.2	4.3	218.5	3.9	218.1	3.7	218.7	3.5	221.1	3.3
60	218.2	5.5	219.2	6.1	218.3	6.0	217.6	5.9	217.8	5.9	218.8	5.5	222.0	4.6
70	214.4	5.8	213.7	7.2	213.3	7.5	213.6	7.9	214.4	8.1	217.5	6.9	222.9	5.4
80	211.1	4.7	209.3	5.9	209.3	6.3	210.0	7.2	211.2	7.8	215.6	7.1	222.9	6.1

Mean temperature ($\overline{T}$) and standard deviation (σ) for June 1997.
Units: Kelvin (K).

λ	350 K $\overline{T}$	σ	380 K $\overline{T}$	σ	400 K $\overline{T}$	σ	435 K $\overline{T}$	σ	475 K $\overline{T}$	σ	550 K $\overline{T}$	σ	675 K $\overline{T}$	σ
40	215.9	5.9	214.0	4.3	212.8	3.5	212.5	2.7	213.7	2.0	217.4	1.1	224.0	0.7
50	219.8	5.4	221.3	4.1	220.5	3.1	219.5	2.3	219.7	2.0	221.3	1.4	226.7	0.8
60	222.5	5.1	225.1	3.6	224.3	2.7	223.4	2.0	223.7	1.6	224.7	1.1	229.4	0.9
70	226.5	4.6	228.9	3.3	228.0	2.5	227.1	1.7	227.7	1.4	228.4	1.1	232.0	0.8
80	228.3	3.7	230.5	2.4	229.9	1.9	229.5	1.4	230.3	1.1	230.6	0.9	233.7	0.7

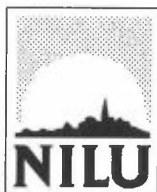Mean temperature ($\overline{T}$) and standard deviation (σ) for September 1997.
Units: Kelvin (K).

λ	350 K $\overline{T}$	σ	380 K $\overline{T}$	σ	400 K $\overline{T}$	σ	435 K $\overline{T}$	σ	475 K $\overline{T}$	σ	550 K $\overline{T}$	σ	675 K $\overline{T}$	σ
40	218.6	7.0	210.5	5.0	209.7	4.1	210.9	2.9	213.1	2.2	217.6	1.5	222.7	1.3
50	219.9	6.4	219.2	5.5	218.2	4.6	217.9	3.5	218.1	3.1	219.3	2.4	222.6	2.3
60	221.5	5.1	222.9	4.4	222.1	3.8	221.6	3.3	221.0	3.1	220.0	2.7	221.6	3.0
70	222.6	4.0	224.8	3.3	224.2	2.7	223.5	2.3	222.3	2.3	222.3	2.3	220.0	3.3
80	225.3	4.2	227.8	3.1	227.0	2.6	225.2	2.5	223.2	2.8	220.8	2.8	219.1	3.3

Mean temperature ($\overline{T}$) and standard deviation (σ) for December 1997.
Units: Kelvin (K).

λ	350 K $\overline{T}$	σ	380 K $\overline{T}$	σ	400 K $\overline{T}$	σ	435 K $\overline{T}$	σ	475 K $\overline{T}$	σ	550 K $\overline{T}$	σ	675 K $\overline{T}$	σ
40	214.7	6.0	214.8	5.0	214.2	4.5	213.7	4.1	213.9	4.3	215.9	4.4	218.1	4.5
50	217.2	6.5	218.0	5.9	217.7	6.1	216.9	7.1	216.3	8.3	215.5	10.3	216.0	11.2
60	217.8	6.6	217.9	7.3	217.3	8.2	216.1	10.3	215.0	12.0	212.2	15.1	211.9	17.7
70	215.9	6.4	215.4	7.6	214.7	8.7	213.5	10.8	212.0	12.7	209.0	15.9	208.9	19.6
80	214.2	4.3	212.3	5.0	211.7	5.9	210.7	7.6	208.6	9.4	206.8	12.4	208.0	16.6

Norwegian Institute for Air Research (NILU)
P.O. Box 100, N-2027 Kjeller – Norway

REPORT SERIES	REPORT NO. OR 11/98	ISBN 82-425-1045-8
SCIENTIFIC REPORT		ISSN 0807-7207

DATE	SIGN.	NO. OF PAGES	PRICE
24 August 1999	Øystein Hov	60	NOK 90.-

TITLE	PROJECT LEADER
Modelling of heterogeneous chemistry in the stratosphere	
	NILU PROJECT NO.
	U-95087/N-97107

AUTHOR(S)	CLASSIFICATION *
Inga Fløisand	A
	CONTRACT REF.

REPORT PREPARED FOR:
European Commission   The Research Council of Norway
DG XII, Science, Research and Development   Miljø og utvikling
Environment and Climate   P.O. Box 2700 St. Hanshaugen
Square de Meeus, 8   N-0131 OSLO
B-1050 BRUSSELS

ABSTRACT
A photochemical trajectory model for the stratosphere has been employed at NILU over several years. The model is made up of coupled modules describing atmospheric processes. This report gives a description of the modules and how the processes are parameterised.

In this study, the model has been applied as a box model in order to study in-situ chemical processes and ozone loss at middle and high northern latitudes in the lower stratosphere. The impact of heterogeneous chemical reactions facilitated by liquid sulphuric acid particles has been investigated. Two different scenarios for particle abundance have been used. The effect of well-established heterogeneous reactions on the partitioning of species, ozone loss mechanisms and ozone depletion rates is examined. In addition, some proposed reactions are studied. The difference in ozone column loss has been calculated.

NORWEGIAN TITLE

Modellering av heterogene kjemiske reaksjoner i stratosfæren

KEYWORDS		
photochemical trajectory model	ozone	heterogeneous reactions

ABSTRACT (in Norwegian)
Rapporten gir en beskrivelse av en fotokjemisk trajektoriemodell for stratosfæren. Modellen omfatter prosesser som fotodissossiasjon, gassfase kjemi, dannelse av flytende og faste partikler og heterogene reaksjoner i forbindelse med disse. I denne studien anvendes modellen som en boksmodell og effekten av heterogene reaksjoner på og i flytende svovelsyre partikler blir studert.

* Classification   A   Unclassified (can be ordered from NILU)
                              B   Restricted distribution
                              C   Classified (not to be distributed)